Multiscale model of dynamic neuromodulation integrating neuropeptide induced signaling pathway activity with membrane electrophysiology

Hirenkumar K. Makadia[1,†], Warren D. Anderson[1,2,†], Dirk Fey[3,†], Thomas Sauter[4], James S. Schwaber[1], and Rajanikanth Vadigepalli[1,*]

[1]Daniel Baugh Institute for Functional Genomics and Computational Biology, Department of Pathology, Anatomy and Cell Biology, Sidney Kimmel Medical College, Thomas Jefferson University, Philadelphia, PA, USA; [2]Graduate program in Neuroscience, Thomas Jefferson University, Philadelphia, PA, USA, [3]Systems Biology Ireland, University College Dublin, Dublin, Ireland; [4]University of Luxembourg, Life Sciences Research Unit, Luxembourg, Luxembourg

Abstract

We developed a novel multiscale model to bridge neuropeptide receptor-activated signaling pathway activity with membrane electrophysiology. Typically, the neuromodulation of biochemical signaling and biophysics have been investigated separately in modeling studies. We studied the effects of Angiotensin II (AngII) on neuronal excitability changes mediated by signaling dynamics and downstream phosphorylation of ion channels. Experiments have shown that AngII binding to the AngII receptor type-1 (AT1R) elicits baseline-dependent regulation of cytosolic Ca^{2+} signaling. Our model simulations revealed a baseline Ca^{2+} dependent response to AT1R activation by AngII. Consistant with experimental observations, AngII evoked a rise in Ca^{2+} when starting at a low baseline Ca^{2+} level, and a decrease in Ca^{2+} when starting at a higher baseline. Our analysis predicted that the kinetics of Ca^{2+} transport into the endoplasmic reticulum play a critical role in shaping the Ca^{2+} response. The Ca^{2+} baseline also influenced the AngII-induced excitability changes such that lower Ca^{2+} levels were associated with a larger firing rate increase. We examined the relative contributions of signaling kinases PKC and CaMKII to AngII-mediated excitability changes by simulating activity blockade individually and in combination. We found that PKC selectively controlled firing rate adaptation whereas CaMKII induced a delayed effect on the firing rate increase. We tested whether signaling kinetics was necessary for the dynamic effects of AngII on excitability by simulating three scenarios of AngII-mediated K_{DR} channel phosphorylation: (1) an increased steady state, (2) a step-change increase, and (3) dynamic modulation. Our results revealed that the kinetics emerging from neuromodulatory activation of the signaling network were required to account for the dynamical changes in excitability. In summary, our integrated multiscale model provides a novel approach for quantitative investigation of neuromodulatory effects on signaling and electrophysiology.

Insert Received for publication Date and in final form Date.

†These authors contributed equally to this work.
*Correspondence: Rajanikanth.Vadigepalli@jefferson.edu
Address reprint requests to Rajanikanth Vadigepalli, Thomas Jefferson University, 1020 Locust Street, Philadelphia PA 19107, USA. Tel.: +1 215-955-0576.
Editor: –

INTRODUCTION

Neuromodulators are integral to the control of intrinsic neuronal excitability, synaptic integration, and neural network function (1–3). Neuromodulators typically interact with specific G protein-coupled receptors (GPCRs) to activate biochemical signaling pathways and alter the metabolism, transcriptional activity, and electrophysiological responsiveness of the postsynaptic cell (4–7). However, the biochemical signaling and electrophysiological responses to neuromodulators have typically been studied separately in computational studies (8). The integration of signaling with electrophysiology in computational

0006-3495/08/09/2624/12 $2.00 doi: 10.1529/biophysj.106.090944

models of non-neuronal excitable cells has yielded important mechanistic insights to the diverse fields including cardiovascular physiology (9, 10), platelet biology (11), and insulin metabolism (12, 13). Our objective for this study was to integrate computational models of signaling pathway activation with those of electrophysiology to study the mechanistic underpinnings of neuromodulation.

We investigated neuromodulatory mechanisms of intracellular signaling and excitability responses to Angiotensin II (AngII) in brainstem neurons. AngII is a peptide neuromodulator involved in the regulation of autonomic nervous system activity via its actions within central autonomic nuclei (6, 14–18). Neuromodulatory effects of AngII are primarily stimulated by the binding of AngII to the type-1 angtiotensin receptor (AT1R) and by eliciting G-protein mediated pathways (19). In brainstem autonomic neurons, AngII influences the inotropic and chronotropic drive of the heart (20, 21). Neurons in autonomic nuclei such as the nucleus of the solitary tract participate in control of cardiovascular regulation at a beat-to-beat time scale and at the level of long term arterial pressure setpoint control (22). Importantly, aberrations of AngII signaling in the brainstem have been implicated in the pathology underlying neurogenic hypertension (23–26). Thus, deciphering the mechanisms of AngII-mediated regulation of neuronal state is central to our understanding of cardiovascular homeostasis and diseases thereof.

Studies of AngII-mediated changes in cytosolic Ca^{2+} levels have shown contrasting effects of AT1R activation on intracellular Ca^{2+} levels, in which both stimulatory and suppressive effects have been reported (27–29). In cultured rat stellate ganglion neurons, it has been demonstrated that this divergence in Ca^{2+} responses was related to the Ca^{2+} baseline level. Suppressive effects were found in neurons with higher Ca^{2+} baseline levels and stimulatory effects were observed in neurons with relatively lower Ca^{2+} baseline levels (27). However, the mechanisms underlying such divergent Ca^{2+} baseline-dependent responses to AngII have not been elucidated. Similarly, it is unclear how this baseline-dependent regulation impacts neuronal excitability. Concomitant with the fluctuations of intracellular Ca^{2+} levels, application of AngII to cultured brainstem neurons *in vitro* results in an AT1R-dependent increase in action potential (AP) firing rate (30–34). Electrophysiological studies have shown that AngII-stimulated PKC and CaMKII activation leads to the phosphorylation of delayed rectifier potassium (K_{DR}) channels, which results in decreased channel conductance and increased firing rate (35–39). The relative contributions of PKC and CaMKII to firing rate response dynamics have not been studied. Our study addresses these mechanistic questions regarding the biochemical basis for divergent Ca^{2+} responses and the molecular contributions to the biophysical consequences of AngII stimulation.

The effects of AngII-mediated neuromodulation result from nonlinear interactions involving numerous elements, thus necessitating a computational approach to unravel the dynamic mechanisms (40, 41). We employed a multiscale modeling approach to quantitatively study AngII-mediated neuromodulation (42–44). We developed an integrated model to bridge GPCR signaling (19) with membrane elctrophysiology (45) through a new biochemical model of ion channel phosphorylation. We examined the molecular contributions to the dynamics of neuromodulation through targeted *in silico* manipulations. Our model incorporated AngII stimulation via Gq receptor activation of the signaling network. Bridging temporal scales from signaling (10 s) to electrophysiology (10^{-3} s) enabled us to investigate AngII/AT1R mediated effects on (1) intracellular Ca^{2+} dynamics, (2) PKC and CaMKII activity and their distinct contributions to downstream neuronal firing, and (3) contributions of dynamic ion channel phosphorylation to firing rate modulation. Our results revealed that controlling the rate of Ca^{2+} transport to ER generated the dichotomy in Ca^{2+} baseline–dependent responses. Examining relative contributions of PKC and CaMKII to excitability changes showed nonlinear interactions among distinct kinase contributions to the dynamics of AngII-mediated neuromodulation. We investigated the importance of dynamic AngII-mediated K_{DR} channel phosphorylation by simulating multiple scenarios of altering K_{DR} channel conductance. We found that that the kinetics of channel phosphorylation were necessary for capturing the dynamics of neuronal excitability. Our multiscale modeling study provides a novel approach to quantitatively investigate the AngII neuromodulatory effects on signaling and electrophysiology, and revealed putative mechanisms underlying the regulation of Ca^{2+} responses, K_{DR} conductance, and neuronal excitability. Understanding the dynamical interactions associated with AngII effects on different Ca^{2+} baseline states and elucidating the differential modulatory effects of kinases on neuronal properties have larger impact in understanding physiology of blood pressure control and pathophysiology of hypertension development (34, 46, 47).

METHODS

An integrated model of neuronal cell signaling and electrophysiology was implemented as a set of ordinary differential equations solved using the ode15s solver in Matlab (Mathworks, USA). The signaling reactions were modeled with either mass-action or Michaelis–Menten kinetics and ion channel electrophysiology was modeled according to the Hodgkin-Huxley formalism. These models were initially validated against their respective data domains independently and were

then integrated to develop a multiscale model of signaling and electrophysiology. The model code in Matlab format and instructions to reproduce the key results are available through accession #156830 in the modelDB resource (48) at http://senselab.med.yale.edu/ModelDB/ShowModel.asp?model=156830

Modeling AngII mediated signaling network dynamics

AngII activated AT1R stimulates phospholipase C (PLCβ) and triggers phosphoinositide (IP) hydrolysis which releases IP3 and DAG, followed by Ca^{2+} mobilization from internal stores and activation of Ca^{2+} dependent enzymes including Protein kinase C (PKC) and Ca^{2+}/Calmodulin dependent protein kinase II (CaMKII) (6). To construct a model of the AngII-mediated signaling network, we started with reaction pathways from an established cellular signaling database (DOQCS, doqcs.ncbs.res.in, accession #31). We employed a model of GPCR-mediated PLCβ activation, IP3 metabolism, Ca^{2+} release by the IP3 receptor (IP3R) in endoplasmic reticulum (ER), and activation of signaling kinases PKC and CaMKII (19) as the basis for our biochemical model. A total of 13 signaling pathways from DOQCS were merged to build the AngII-mediated signaling network (Table S1). Our integrated model comprises of 13 signaling pathways, a biochemical model of ion-channel phosphorylation and an electrophysiological model containing six ion channels. A schematic of the integrated model topology including signaling network is shown in Figure 1A.

We modified the initially collated signaling network in three distinct ways:

1. The DOQCS model of Gq pathway activation was based on metabotropic glutamate receptor (mGluR) signaling. We replaced the mGluR kinetics with those of AngII receptor type 1 (AT1R). The forward rate constant for binding of AngII to AT1R was estimated based on experiments from (49). The corresponding backward reaction kinetics were assumed to be similar to those of mGluR and were obtained from (19). The total AT1R concentration in the model was based on (50). The majority of the parameters were initially taken from the DOQCS resource, as these parameters were tuned based on data from brain tissues (19).

2. We compartmentalized the Ca^{2+} dynamics in the model into three sections: the intracellular (cytosolic), the ER (sequestered), and the peri-membrane space adjacent to calcium channels (extracellular). Cytosolic Ca^{2+} could be either free or buffered and the IP3 receptor regulated its transport from the ER. Reaction details and parameter values for the Ca^{2+} regulation model are shown in Table S2. Parameters corresponding to non-oscillatory Ca^{2+} response were modified to match the experimental data from neurons (27, 29). Table S2 also shows reactions and/or equations for all of sub-modules of calcium dynamics, except for the Ca_L type ion-channel which are reported in Table S3.

3. We augmented the Ca^{2+} regulation module to include the sodium-calcium exchanger (NCX). Electro-diffusion of NCX, characterized by the influx of three Na^+ ions for the efflux of every Ca^{2+} ion, was modeled based on the Goldman-Hodgkin-Katz (GHK) equation (51). The chemical flux component of the exchanger was modeled with a PKC-dependent regulatory component (52, 53), which also incorporated Michaelis-Menten kinetics for allosteric activation by Ca^{2+} (54) (refer sodium-calcium exchanger module in Table S2 for details).

Modeling the neuronal membrane electrical activity dynamics

Neuronal electrophysiology was modeled using a modified Hodgkin and Huxley formalism (55). We modeled it with an electrical circuit (Figure 1B) containing multiple ionic currents balanced across the membrane (see supporting text section S2 for details). The channel conductance and their current expressions for sodium channel (Na^+), delayed rectifier potassium channel (K_{DR}), A-type potassium channel (K_A), L-type calcium channel (Ca_L^{2+}), hyperpolarized calcium dependent potassium channel (K_{AHP}), and a non-specific leak channel are described in Table S3.

The initial parameters of the electrical model were based on the model of cardiorespiratory brainstem neuron (45). The model parameters were modified to match experimental observations of increased firing rates, reduced K_{DR} currents, and increased intracellular Ca^{2+} concentration following AngII application. The following constraints were imposed on the model based on AngII experimental data:

1. The maximal conductances of the different channel types were adopted from (45). This ensured a brainstem neuronal phenotype exhibiting the physiological firing rate at nominal conditions (38).

2. The steady state activation variables of the K_{DR} and K_A currents (i.e., $m_{K_{DR},\infty}$ and $m_{K_A,\infty}$ in Table S3) were chosen to provide a good fit to whole cell patch-clamp data (35, 39).

Modeling ion-channel phosphorylation to bridge signaling pathways and electrical activity

We considered the macroscopic conductance of K_{DR} channel as dependent on phosphorylation by PKC and CaMKII. A new kinetic model was constructed based on mass action kinetics (Figure 1C). Experimental data show that phosphorylation of K_{DR} channels results in a substantial reduction in current (50-90%; (56)). We assumed that phosphorylated K_{DR} channels could be completely inhibited at saturating levels of channel phosphorylation (i.e., $g_{K_{DR}} = 0$). The K_{DR} conductance $\bar{g}_{K_{DR}}$ was obtained by multiplying basal maximal conductance by the fraction of unphosphorylated channels. The phosphorylation reactions were modeled with first order kinetics as:

$$\frac{d\mathrm{K_P}}{dt} = k_p[\mathrm{K_U}][\mathrm{kinase}]^n - k_{dp}[\mathrm{K_P}] \quad (1)$$

$$\mathrm{K_T} = \mathrm{K_U} + \mathrm{K_P} \quad (2)$$

$$\mathrm{K_P} = \mathrm{K_{PKC}} + \mathrm{K_{CaMKII}} + \mathrm{K_{PKC,CaMKII}} \quad (3)$$

where K_T represents the total fraction of potassium channels with n phosphorylation sites ($K_T = 1$), K_U represents the fraction of unphosphorylated channels, and K_P represents the fraction of phosphorylated channels. The levels of phosphorylated channels represent aggregate of channels phosphorylated either by PKC, CaMKII, or both. Kinases were assumed to act independently on distinct phosphorylation sites on these channels. The parameter $n = 4$ was set for simplification under the assumption that each of the four channel subunits can be phosphorylated. In our integrated model, PKC and CaMKII both phosphorylated K_{DR} (see Table S4 for details).

To simulate phosphorylation-mediated reduction of K_{DR} current, we weighted its peak conductance by the fraction of un-phosphorylated channels in Table S3 ($K_U = 1$ before AngII stimulation):

$$I_{K_{DR}}(V) = \mathrm{K_U} \cdot \bar{g}_{K_{DR}} \cdot m^4_{K_{DR}} (V - E_K) \quad (4)$$

To occlude the phosphorylation reactions of a kinase *in silico*, we set $k_{p,CAMKII}$ and/or $k_{p,PKC}$ in Table S4 to zero.

RESULTS

Bridging the signaling network with the electrophysiology model

Bi-directional interactions between the signaling and electrophysiological domains arise due to (1) kinases PKC and CaMKII phosphorylating the K_{DR} channel, (2) the dependence of NCX on membrane potential, (3) the contribution of voltage-dependent Ca^{2+} channels to Ca^{2+} regulation, and (4) the effects of Ca^{2+} level on Ca^{2+} dependent potassium channel conductance (K_{AHP}). The signaling network model was modified to incorporate the membrane potential as a dynamic state variable in the NCX description. The maximal conductance of K_{DR} was dependent on the state variables corresponding to active PKC and CaMKII as detailed above. The remaining key interactions involved Ca^{2+} dynamics due to release from cytosolic stores in the signaling model and flux through ion channel currents in the electrical model.

Simulations indicated that the Ca^{2+} levels affecting K_{AHP} had to be considered separately from the levels of free cytosolic Ca^{2+}. Otherwise, large increase in cytosolic Ca^{2+} levels following AngII stimulation activated the K_{AHP} current to saturation and prevented any neuronal firing activity. The hypothesis that there exists a peri-membrane Ca^{2+} compartment distinct from bulk cytosolic Ca^{2+} is supported by experimental data (57) and is typically considered as such in neuronal modeling studies (58). To address this issue, Ca^{2+} dynamics were compartmentalized in the model such that the K_{AHP} and Ca_L channels were assumed to be closely situated with local Ca^{2+} buffering and were uninfluenced by bulk cytosolic Ca^{2+}.

Integrated AngII signaling and electrophysiology model accounts for the dynamics of K_{DR} channel phosphorylation

Our integrated model quantitatively simulated AngII/AT1R-mediated neuromodulation by recapitulating experimental findings from brainstem neurons. To fit the electrophysiological data with that of signaling network interactions, we varied the ratio of (K_{DR}) phosphorylation to dephosphorylation rate constants (k_p/k_{dp}) for PKC and CaMKII (Figure 1D). The model was calibrated to account for the 30% reduction in K_{DR} current observed following application of 100 nM AngII (37). Evidence suggests that this current reduction is attributable to K_{DR} channel phosphorylation (37). We then tuned the k_p and k_{dp} parameters for PKC and CaMKII that rendered the 30% reduction in the fraction of un-phosphorylated K_{DR} channels. This calibration recapitulated the kinetics of K_{DR} current reduction following the application of 100 nM AngII (Figure 1E), as well as the shift in the K_{DR} current-voltage relation observed in voltage-clamp data (Figure 1F) (37). Our results showed that

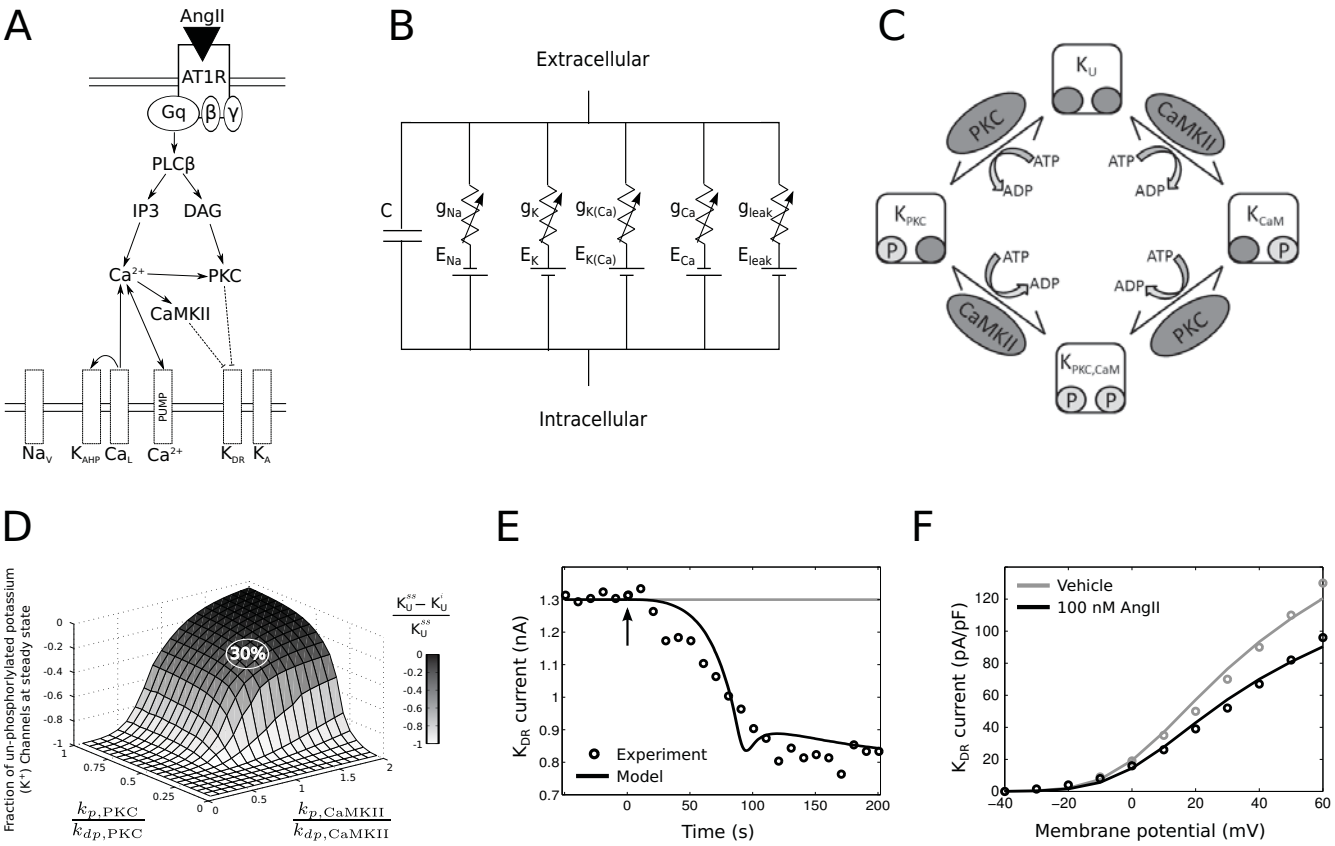

Figure 1: **Integrated model of the intracellular signaling and electrophysiology.** (A) An overview of the integrated model topology, showing AngII activation eliciting multiple signaling pathways and subsequently modulating membrane electrophysiology. (B) Circuit diagram of the electrophysiology model. (C) Schematic depicting the phosphorylation reactions underlying the AngII-mediated reduction of K_{DR} conductance. (D) Plot showing the fractional reduction of un-phosphorylated K_{DR} channels as a function of phosphorylation / de-phosphorylation reaction rate ratios $\left(k_p/k_{dp}\right)$ for both PKC and CaMKII. Data correspond to simulations in which K_U^{ss} indicates the fraction of un-phosphorylated K_{DR} channels following 100 nM AngII at steady state and K_U^i refers to the fraction of unphorphorylated K_{DR} channels before the application of AngII. The relative phorphorylation and dephosphorylation rates were set to yield approximately 30% reduction in un-phosphorylated channels to fit the experimental data in panel E (See Table S4 for reaction details). (E) Model fit to dynamic K_{DR} current data following the application of 100 nM AngII to cultured brainstem neurons (37). (F) I-V relations for K_{DR} from experiments (37) and simulations under baseline conditions and following 100 nM AngII application to cultured brainstem neurons.

the combined effects of PKC and CaMKII were required to attain the experimental results. The fitted CaMKII rate constants were equal for phosphorylation and dephosphorylation and the PKC dephosphorylation rate constant was twice that of the PKC phosphorylation rate constant. Our integrated model with known signaling network interactions, when appropriately tuned with channel phosphorylation kinetics, accounted for the experimentally observed dynamics of excitability changes in response to AngII stimulation.

Ca^{2+} baseline-dependent bifurcation of signaling responses to AngII

AngII application resulted in a dose-dependent AT1R-signaling pathway response, including regulation of PKC and CaMKII by Ca^{2+}. Cytosolic Ca^{2+} levels in neurons are maintained by chemical and electrochemical fluxes due to L-type Ca^{2+} channels (Ca_L), the sodium-calcium exchanger (NCX), and plasma membrane Ca^{2+} pumps (EPump) (See Figure 2A). Excess intracellular Ca^{2+} is stored in the ER until the buffer reaches its saturating limit, and is released following IP3R binding. Experimental observations have shown that AngII elicits divergent neuronal responses depending on Ca^{2+} baseline levels (see insets in Figure 2D and F) (27). To determine why such divergent responses occur, we individually varied all of the parameters in the Ca^{2+} regulation module to search for variations that could reproduce this nonlinear behavior. We found that reducing the rate of Ca^{2+} transport into the ER ($k_{\mathrm{ER}}^{\mathrm{Ca}^{2+}}$) increased the cytosolic Ca^{2+} baseline levels at steady state without AngII (Figure 2B), thus

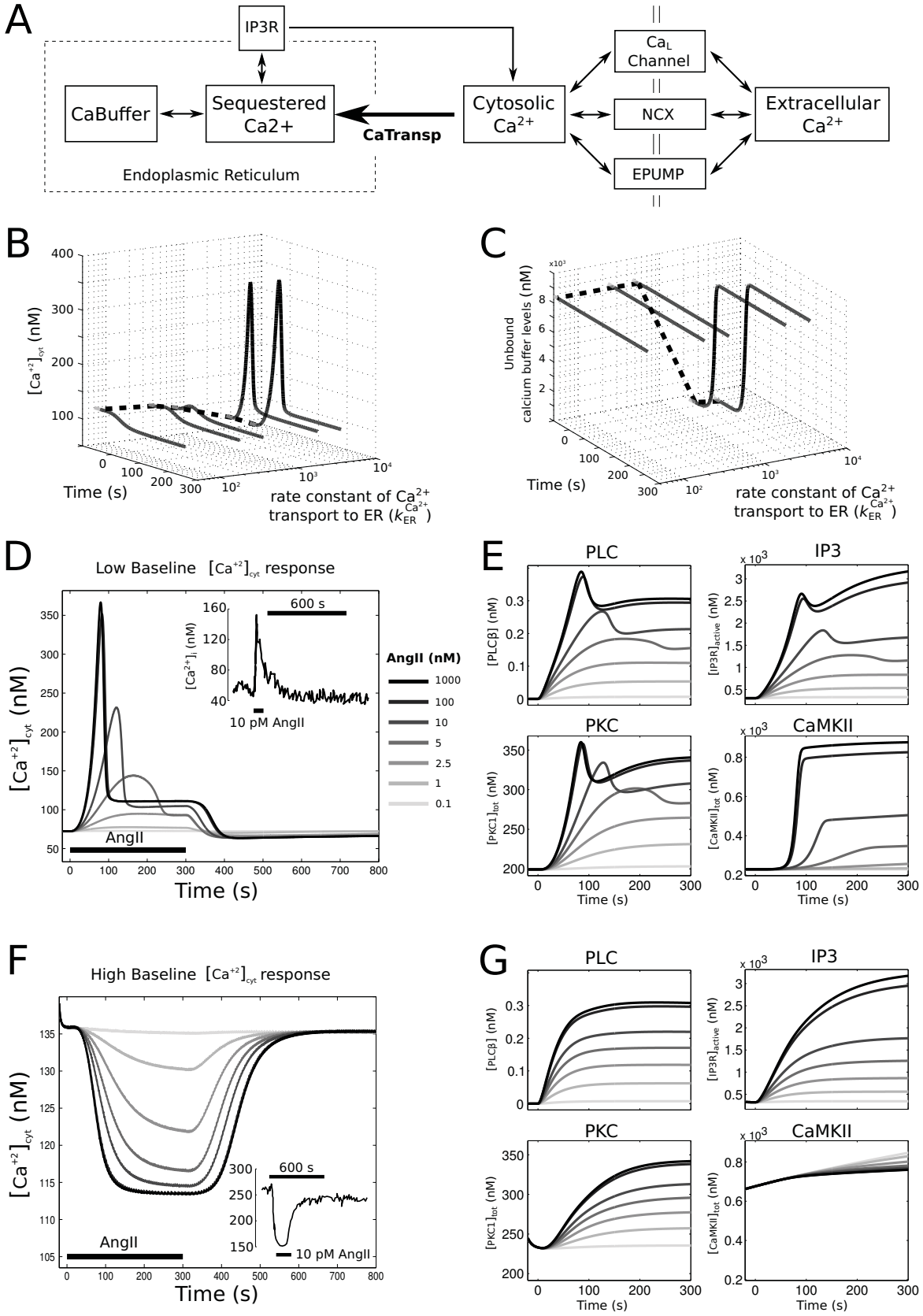
A
IP3R
CaBuffer
Sequestered Ca2+
CaTransp
Cytosolic Ca2+
Ca_L Channel
NCX
EPUMP
Extracellular Ca2+
Endoplasmic Reticulum
B
[Ca+2]cyt (nM)
Time (s)
rate constant of Ca2+ transport to ER (k_ER^Ca2+)
C
Unbound calcium buffer levels (nM)
Time (s)
rate constant of Ca2+ transport to ER (k_ER^Ca2+)
D
Low Baseline [Ca+2]cyt response
[Ca+2]cyt (nM)
[Ca2+]i (nM)
600 s
10 pM AngII
AngII
AngII (nM)
1000
100
10
5
2.5
1
0.1
Time (s)
E
PLC
IP3
PKC
CaMKII
[PLCβ] (nM)
[IP3R]active (nM)
[PKC1]tot (nM)
[CaMKII]tot (nM)
Time (s)
F
High Baseline [Ca+2]cyt response
[Ca+2]cyt (nM)
600 s
10 pM AngII
AngII
Time (s)
G
PLC
IP3
PKC
CaMKII
[PLCβ] (nM)
[IP3R]active (nM)
[PKC1]tot (nM)
[CaMKII]tot (nM)
Time (s)

Figure 2 (previous page): **Nonlinear baseline Ca^{2+}-dependent response to AngII stimulus, in which low cytosolic Ca^{2+} baseline levels resulted in an increase in cytosolic Ca^{2+} and high cytosolic Ca^{2+} levels resulted in a decrease in cytosolic Ca^{2+} levels.** (A) Schematic of Ca^{2+} regulatory dynamics. (B) Dynamic traces of cytosolic Ca^{2+} as a function of change in the rate constant of Ca^{2+} transpor into the ER ($k_{\mathrm{ER}}^{\mathrm{Ca}^{2+}}$). Solid black lines indicate the time period where 100 nM AngII was applied whereas solid gray lines indicate steady state levels preceding AngII application. Decreasing the $k_{\mathrm{ER}}^{\mathrm{Ca}^{2+}}$ from 3600 to 36 $\mu\mathrm{M}^{-2}\mathrm{s}^{-1}$ increases the Ca^{2+} baseline levels from approximately 72 to 136 nM (dotted line). (C) Dynamic traces of unbound calcium buffer levels as a function of change in $k_{\mathrm{ER}}^{\mathrm{Ca}^{2+}}$. For plot details, see (B). Decrease in $k_{\mathrm{ER}}^{\mathrm{Ca}^{2+}}$ drains out all stored Ca^{2+} in the buffer prior to AngII application (Total capacity of the saturated buffer = 9091 nM). (D) AngII dose-dependence of cytosolic Ca^{2+} response for low cytosolic Ca^{2+} baseline condition. Inset, top right panel shows the intracellular calcium tracing from primary cultures of neonatal rat sympathetic neurons when exposed to 3 min AngII pulses (10 pM) for low baseline condition (27). (E) Upstream responses of PLCβ and active IP3R (IP3-bound IP3R), and downstream kinase responses of PKC and CaMKII for the low Ca^{2+} baseline condition. (F) AngII dose-dependence of cytosolic Ca^{2+} response for high cytosolic Ca^{2+} baseline condition. Inset, bottom right panel shows the intracellular calcium tracings taken from cells (see (D) for details) with a higher baseline (greater than 200 nM). (G) High Ca^{2+} baseline condition upstream responses of PLCβ and active IP3R, and downstream kinase responses of PKC and CaMKII.

instantiating the high baseline Ca^{2+} condition. Reduction in this rate constant (from 3600 to 36 $\mu\mathrm{M}^{-2}\mathrm{s}^{-1}$) initiates an efflux of all stored Ca^{2+} from the ER to the cytosol. This efflux resulted in an empty ER buffer in the high Ca^{2+} baseline condition (Figure 2C). This is because the decreased influx rate of Ca^{2+} into the ER induced an imbalance in Ca^{2+} flux between ER and cytosol. Since the outward rate (3125 $\mu\mathrm{M}^{-1}\mathrm{s}^{-1}$) remained the same, the increase in rate difference (outward vs. inward) introduced a driving force that favored Ca^{2+} extrusion from ER. At steady state the ER Ca^{2+} buffer transferred all of its sequestered Ca^{2+} into the cytosolic region, resulting in an increase in the intracellular Ca^{2+} baseline level. Additionally, most of the Ca^{2+} that entered cytosol was quickly moved to the extracellular region in order to maintain intracellular equilibrium. Thus, due to a change in the amount of Ca^{2+} available in ER store for different Ca^{2+} baseline conditions, application of AngII led to a divergence in cytosolic Ca^{2+} and buffer responses to AngII.

AngII was applied to a neuronal state that was characterized by a higher rate of Ca^{2+} transport into ER, or the corresponding low cytosolic Ca^{2+} baseline condition. Our simulations resulted in an increase in cytosolic Ca^{2+} level followed by a response adaptation. The Ca^{2+} level returned to the initial baseline state after withdrawal of AngII (Figure 2D). The peak Ca^{2+} response increased nonlinearly as a function of AngII dose (Figure 2D). The time point of the initial Ca^{2+} peak after stimulation was observed within approximately 45 s in stellate ganglion cells (27). Our simulation results showed an initial peak within 50-120 s and thus provided a good match to these data in terms of the observed time response. The absolute peak values were comparable in both experimental data sets and were matched well by the model. For AngII concentrations up to 1 nM the Ca^{2+} response was negligible, though the response increases sigmoidally for AngII >1 nM (Figure S2A). The dynamics of PLCβ, IP3, PKC, and CaMKII exhibited saturating responses with distinct amplitudes and kinetics (Figure 2E). PLCβ and bound IP3R showed peak responses followed by either sustanined or transient adaptations, respectively. PKC showed a peak response followed by adaptation, whereas CaMKII, which is activated solely by Ca^{2+}, showed a relatively delayed increase without adaptation. The CaMKII responses showed initial kinetics and a dose-response relation similar to that of Ca^{2+}, while other species showed a markedly reduced kinetics and cooperativity (Figure 3). These results are in agreement with experimental results from (59). Simulations with a higher Ca^{2+} baseline indicated that Ca^{2+} decreased significantly after AngII stimulation, but returned to the initial steady state levels after withdrawal of AngII (Figure 2F). For high baseline condition, PLCβ, IP3, and PKC showed increases in their levels following AngII stimulation but showed saturated response at high AngII doses (Figure 2G). The CaMKII response, however, displayed a decrease in levels as it was activated solely by intracellular Ca^{2+}.

We examined the dose-dependency of AngII-mediated peak Ca^{2+} response for the high and low Ca^{2+} baseline conditions. Hill equation fits for the high Ca^{2+} baseline condition yielded a lower $K_{0.5}$ compared to that of the low Ca^{2+} baseline (Figure 3A). This suggests that there is differential sensitivity to AngII for the high versus low Ca^{2+} baseline. We fitted Hill equations to both peak and steady state (t = 300 s) AngII dose-response relations for PLCβ, IP3, PKC, and CaMKII (Figure 3B and Table S5). The results showed similar dose response profiles for PLCβ, IP3, and PKC in the high and low Ca^{2+} baseline conditions. This similarity trend was obtained for both the peak and steady state responses of PLCβ, IP3, and PKC (Table S5). In contrast, the deactivation of CaMKII following AngII application to the high Ca^{2+} baseline condition had a lower $K_{0.5}$ compared to the low baseline condition. This suggests that the deactivation of CaMKII in the high Ca^{2+} baseline condition is more sensitive to AngII concentration when compared to the activation of CaMKII in the low Ca^{2+} baseline condition. Although active PKC levels were elevated in the high Ca^{2+} baseline condition, the responsiveness of PKC to AngII stimulation was similar in both Ca^{2+} baseline conditions. However, while the changes in CaMKII levels were relatively small in the high Ca^{2+} baseline condition, the AngII dose-dependence of CaMKII deactivation relation was left-shifted compared to the low Ca^{2+} baseline condition. Further, we found that the baseline firing rate were elevated in the high Ca^{2+} baseline

state (Figure S2). This increase in baseline firing rate was due to increase in baseline CaMKII levels, and application of AngII induced a slow and small change in excitability resulting in a comparable electrophysiological state as that of the low Ca^{2+} baseline state (see details in supporting text section Section S3).

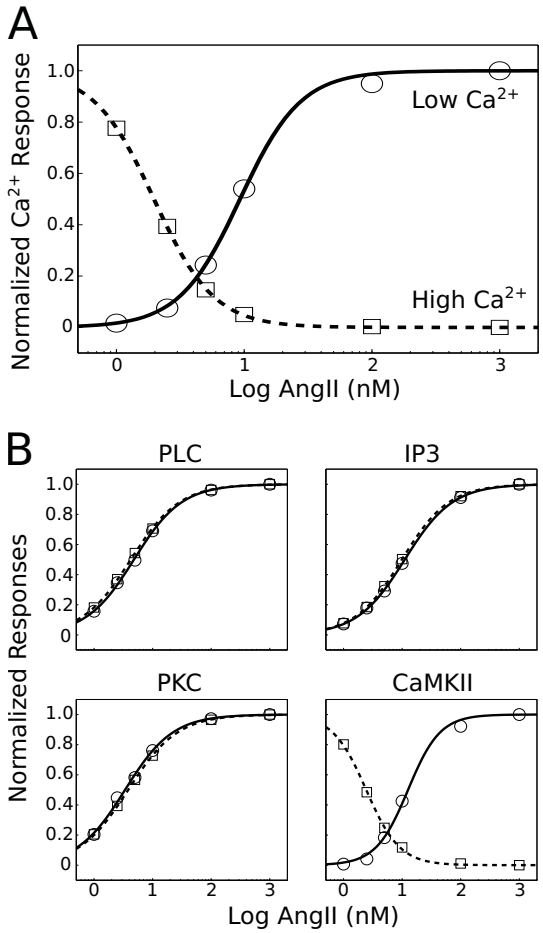

Figure 3: **AngII dose-dependence of divergent Ca^{2+} responses.** (A) Baseline-subtracted peak deflections were normalized and plotted for high and low Ca^{2+} baseline phenotypes. Dose-response data were fitted with the Hill equation: $[\mathrm{AngII}]^{n_H}/([\mathrm{AngII}]^{n_H} + K_{0.5}^{n_H})$. Fit results indicate that the high Ca^{2+} baseline phenotype is more sensitive to AngII as compared to that of the low Ca^{2+} baseline phenotype ($K_{0.5} = 2.0$ nM and $K_{0.5} = 9.3$ nM, respectively). However, the cooperativity coefficients were nearly identical ($n_H = 1.85, 1.82$). (B) steady state responses ($t = 300$ s) of PLC, IP3, PKC, and CaMKII were baseline-subtracted, normalized, and fitted as described above. Dose-response relations for PLC, IP3, and PKC were nearly identical for the high- and low- Ca^{2+} baseline phenotypes (see Table S4 for all fit parameters). Because CaMKII is activated by cytosolic Ca^{2+}, active CaMKII levels decrease along with Ca^{2+} in the high baseline condition. The AngII-dependence of the CaMKII response is pronounced in the high baseline phenotype relative to the low Ca^{2+} baseline condition ($K_{0.5} = 2.4$ nM and $K_{0.5} = 12.6$ nM, respectively), while the cooperativity coefficients were similar ($n_H = 1.52, 1.59$). Dose response relations for peak responses yielded similar trends (Table S4).

Distinct dynamic contributions of CaMKII and PKC to AngII–mediated changes in neuronal excitability

To examine the relative contributions of PKC- and CaMKII-mediated phosphorylation of K_{DR} channels to AngII-mediated firing rate responses, we simulated '*in silico* blockade' of each phosphorylation mechanism by removing the corresponding reactions from the model individually and in combination (Figure 4A). Such scenarios are biologically plausible if the phosphorylation sites are unavailable due to genetic polymorphisms with potential therapeutic implications (60). The wildtype simulation (Figure 4B, condition 1) showed an excitability increase following AngII stimulation that exhibited adaptation in the continuous presence of AngII. Occluding PKC-dependent channel modulation (Figure 4B, condition 2) significantly altered the response to result in a faster, but delayed, increase in firing rate without adaptation. Blocking CaMKII-dependent phosphorylation (Figure 4B, condition 3) had an effect on overall gain but not on the pattern of neuronal adaptation. Blocking modulation by both kinases (Figure 4B, condition 4) abrogated the AngII-mediated increase in neuronal excitability. These

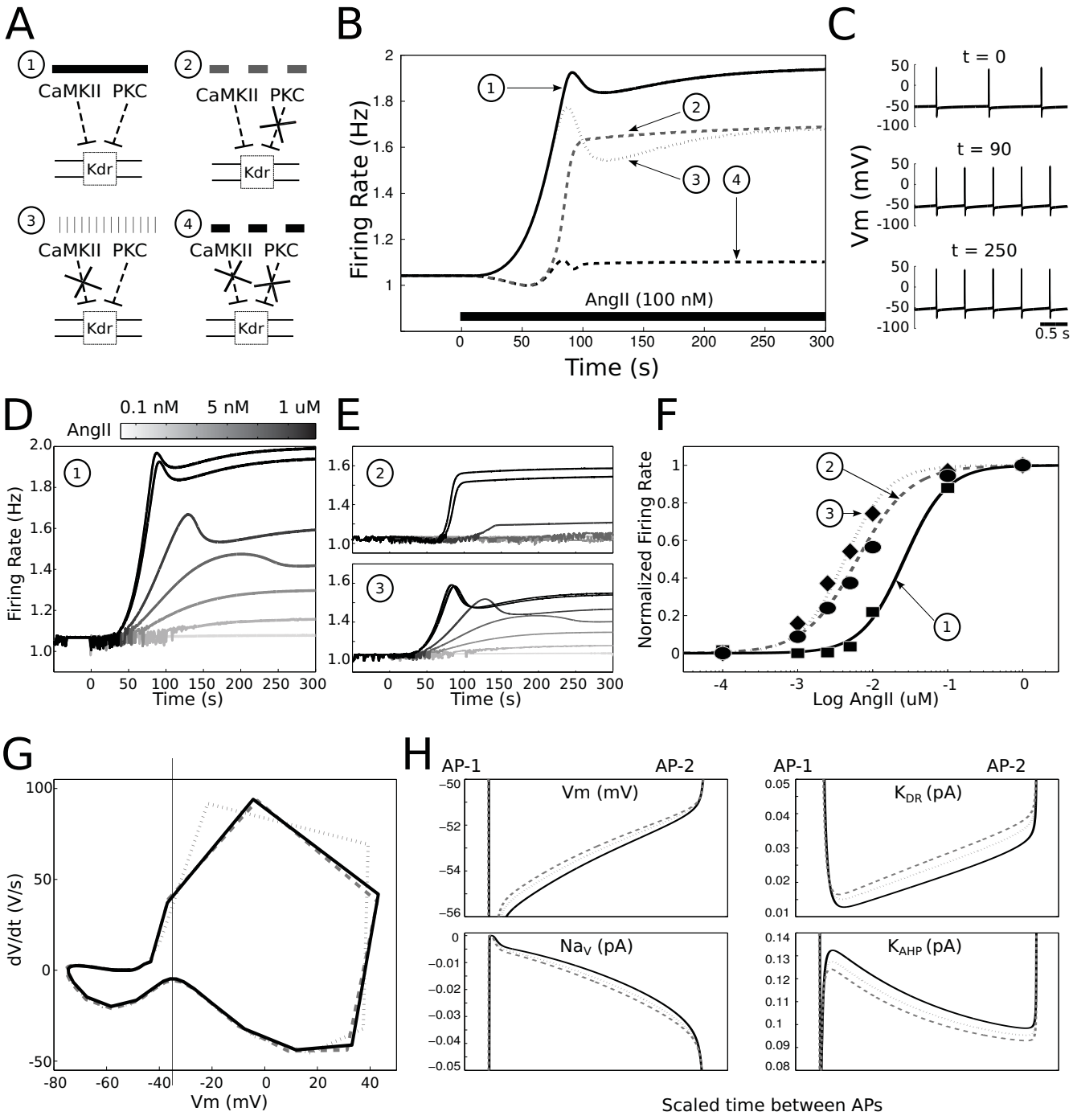

Figure 4: **Distinct dynamic contributions of PKC and CaMKII to AngII-mediated excitability changes.** (A) The neuronal response to AngII was simulated in four conditions: (1) the wildtype reference simulation, (2) occluding PKC phosphorylation of K_{DR}, (3) occluding CaMKII phosphorylation of K_{DR}, and (4) occluding both CaMKII and PKC-mediated phosphorylation of K_{DR}. (B) Firing rate responses to 100 nM AngII (starting at $t = 0$ s) are shown for all four conditions. (C) Membrane potential time-series at $t = 0, 90, 250$ s showing increases in excitability following AngII application to the wildtype model (1). (D-E) Responses at a range of AngII input levels are shown for the wildtype and single kinase phosphorylation occusion conditions (1-3). (F) Baseline-subtracted firing rate responses at steady state ($t = 300$ s) are plotted as a function of AngII concentration for conditions 1-3. Each relation was fitted with a Hill equation: $[\mathrm{AngII}]^{n_H}/([\mathrm{AngII}]^{n_H} + K_{0.5}^{n_H})$. (G) Phase-space representations of APs at the times of peak responses to AngII for conditions 1-3 (same legend as in panels B,F). (H) Inter-spike interval biophysical properties of conditions 1-3 at times of peak responses to AngII. Abbreviations: Vm = membrane potential,Na_V = Na^+ current, K_{DR} = K_{DR} current, K_{AHP} = K_{AHP} current.

results indicate that NCX alone does not influence the neuronal firing rate under the conditions of our simulations, whereas CaMKII and PKC have distinctive effects on the dynamics of neuronal firing rate responses to AngII stimulation. Both conditions of kinase phosphorylation occlusion resulted in similar steady state firing rates that were approximately 75% of the wildtype response, indicating a nonlinear interaction among kinases.

We next investigated the dose-response effects of AngII on excitability (Figure 4D–F). We applied a range of AngII doses and fitted Hill equations to the rate versus dose relations at peak and at steady state (Table S6). The results for steady state fits showed that the wildtype phenotype (1) had a reduced sensitivity to AngII when compared to the individual *in silico* blockade conditions (1,2), both of which showed similar sensitivities to AngII (Figure 4F). These results suggest that pronounced reductions in the activity of either kinase individually will reduce the excitability response amplitude but increase the sensitivity to AngII. Results for fits to peak firing rates showed similar trends (see Table S6 and Figure S4). While firing rates were different at the times of peak responses in conditions 1-3, AP waveforms were similar indicating the absence of K_{DR} phosphorylation effects on AP threshold or repolarization (Figure 4G). To interrogate the electrophysiological basis for the observed effects, we examined the ionic contributions to the AngII firing rate responses in conditions 1-3 at times of peak AngII responses in each respective condition. The results showed that occluding phosphorylation of K_{DR} led to subtle changes in Na^+, K_{AHP}, and K_{DR} currents during inter-spike intervals (Figure 4H). This suggests that differences in K_{DR} phosphorylation, as determined by the relative contributions of PKC and CaMKII, alter the contributions of other ionic conductances and thereby modify the overall electrophysiological response to AngII stimulus.

Kinetic channel modulation is required to account for the dynamics of AngII–mediated excitability changes

We hypothesized that the kinetics of AngII signaling pathway activation are required to shape the dynamic response profile. To test this hypothesis, we evaluated the electrophysiological response under three distinct K_{DR} phosphorylation conditions: (1) higher steady state phosphorylation, (2) step change to instantaneously increased phosphorylation, and (3) signaling kinase mediated dynamic changes in phosphorylation (Figure 5A). The results showed that a steady state reduction of K_{DR} conductance produced a constant firing rate (Figure 5B). A step reduction in K_{DR} conductance produced a transient excitability increase followed by a constant firing rate. The dynamic profile of the firing rate change due to kinetic signaling activity was strikingly different from those elicited by steady state and well as step changes in K_{DR} phosphorylation (Figure 5B). Hence, we conclude that the signaling kinase-mediated phosphorylation of K_{DR} is required to reproduce the dynamics of the experimentally observed neuronal response to AngII stimulation (Figure 1E).

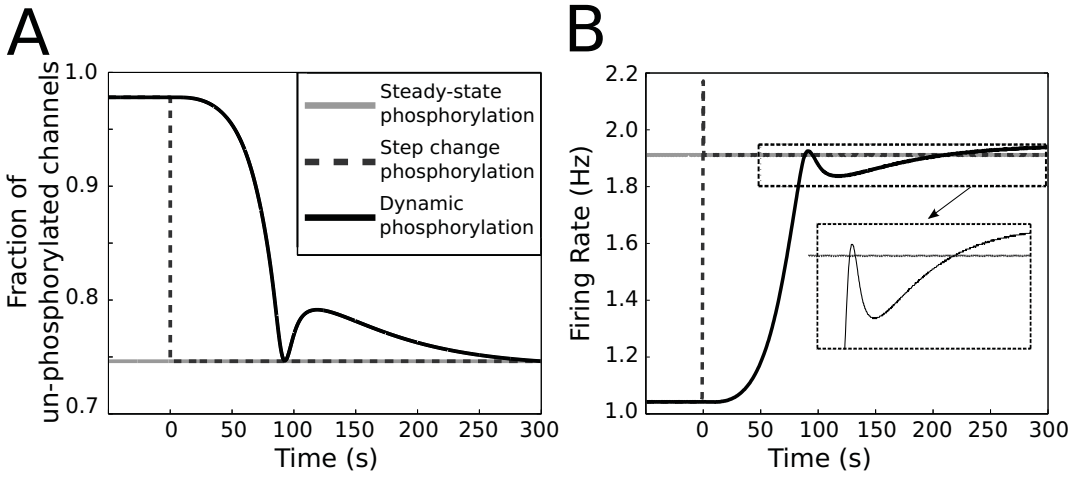

Figure 5: **Dynamic K_{DR} channel modulation emerging from signaling activities is necessary to account for the dynamics of AngII induced neuronal excitability.** (A) Simulated fractions of un-phosphorylated K_{DR} channels for three scenarios describing AngII-mediated K_{DR} channel phosphorylation: (1) a steady state increase, (2) a step-change increase, and (3) dynamic modulation. (B) AngII induced firing rate responses (100 nM starting at $t = 0$ s) for the three simulated scenarios. The inset highlights the distinct effects of dynamic phosphorylation corresponding to scenario (3) as compared to those of non-dynamic phosphorylation (scenarios 1 and 2).

DISCUSSION

Neuromodulation is a subject under intense investigation in experimental and computational neuroscience given its role in a plethora of physiological, behavioral, and cognitive functions of the central/peripheral nervous systems in health and disease (1–3, 61–63). The present work integrates a large scale biochemical signaling network with a detailed Hodgkin-Huxley-like model of membrane electrophysiology to study dynamic neuromodulation. While biochemically detailed models have been developed that incorporate neuromodulator induced signaling influences on specific ion channels, these models do no contain a cadre of ion channels sufficient for suprathreshold membrane potential dynamics and action potential firing (64–66). Models have been developed that integrate temporal and spatial scales of calcium dynamics and multiple channels in dendrites to investigate mechanisms underlying synaptic plasticity (42–44, 67–69). Some models of cardiac physiology incorporated GPCR-mediated modulation of signaling cascades (9, 10), while others either do not include GPCRs or simulate their effects as steady state parameter changes (70–72). In addition, the majority of the published neuromodulation models have simulated the modulatory influences on electrophysiology with steady state parameter variations, whereas only some models have included kinetics based on coarse-grained abstractions of the underlying cell signaling pathways (8). A quantitative study of neuromodulation, therefore, must integrate GPCR-neuropeptide interactions, biochemical signaling pathways, calcium dynamics, and membrane electrophysiology to thoroughly interrogate the underlying dynamical interactions (40, 41). Because signaling events evolve over seconds and electrophysiological dynamics span milliseconds, integrative modeling of neuromodulation necessitates the bridging of time scales. It also entails signaling events that span multiple spatial components, from organelle to cell. Thus, we developed a multiscale modeling approach to study neuromodulation in the context of AngII-mediated influences on brainstem neurons.

Our model captured two distinct experimentally observed divergent AngII-mediated response patterns. AngII elicits a cytosolic Ca^{2+} increase at low baseline Ca^{2+} levels and a Ca^{2+} decrease at high baseline Ca^{2+} levels (27). Effects of intracellular Ca^{2+} diffusion particularly during its transport to and from ER have been noted in oscillatory Ca^{2+} releases (73). However, Ca^{2+} diffusion within the cell cytoplasm is much slower compared to transport due to secondary messenger such as IP3 (74). Since our model contains non-oscillatory Ca^{2+} mobilization, we considered that the flux due to Ca^{2+} diffusion has minimal effect in comparison to the fluxes of channels/pumps, and ignored the former component in the present model. Further analysis of the simulation results revealed that the decrease in cytosolic Ca^{2+} can be explained by reducing the rate constant of Ca^{2+} flux into the ER. These results suggest that the signaling system is re-calibrated in conditions of high Ca^{2+} such that the ER Ca^{2+} stores are completely eliminated. This finding indicated that the augmentation of Ca^{2+} baseline levels elevated baseline neuronal firing frequency but diminished the changes in AngII-induced excitability. These observations are consistent with data showing that repeated applications of AngII lead to tachyphylaxis (75, 76). The Ca^{2+} baseline-dependence of AngII-mediated responses is also consistent with the observation that AngII elicits divergent effects on blood pressure *in vivo* via actions within the rostral brainstem (77). Such alterations of Ca^{2+} responses may have important implications for AngII-mediated effects on gene expression and gene regulatory influences on autonomic control of cardiovascular physiology (78, 79).

Pharmacological studies have implicated a definitive role of PKC and CaMKII in the modulation of various ion channels. In particular, the delayed rectifier potassium (K_{DR}) current decreases upon AT1R activation by AngII in brainstem neurons (35–39). The inhibition of K_{DR} current is believed to occur following direct phosphorylation of Kv2.2 subunits (35, 36). While it is still unclear whether direct phosphorylation of Kv2.2 occurs, Kv2.1 channels have been shown to be directly phosphorylated (80). Inhibition of K_A has also been shown to occur following direct phosphorylation of the Kv1.4-a subunit at putative PKC and CaMKII sites (81). However, we found that inhibition of K_A current did not alter firing rate significantly relative to changes in K_{DR} conductance in our model. Hence, we did not simulate kinase mediated phosphorylation reactions with K_A channels. Our assessments of the relative contributions of PKC and CaMKII to AngII-mediated modulation of firing rate showed that these kinases reduced the neuronal sensitivity to AngII. The steady state excitability response to saturating AngII doses is largely intact in the complete absence of either of the kinases, suggesting a high degree of redundancy in the dual kinase system within our model. The kinetic contributions of each kinase is also distinct such that PKC determines the initial response kinetics and firing rate adaptation, whereas CaMKII contributes exclusively to firing rate gain while reducing the extent of adaptation. Overall, our simulations suggest that PKC and CaMKII fine tunes the degree, timing, and adaptation of excitability responses to AngII. Our simulation results could be experimentally tested via targeted perturbations of these kinases in brainstem cardiac control regions which could ameliorate the aberrant effects of AngII on sympathetic overdrive observed in conditions such as hypertension and heart failure (21).

Molecular neuronal pathways elicited by AngII binding to AT1R in brainstem neurons are involved in the regulation of blood pressure and development of hypertension (14, 82–84). These activated pathways include both that trigger short term increase

in neuronal firing rate, and those that affect gene expressions and protein levels for longer term effects leading to sustained changes in neuronal activities (6, 33, 85, 86). Our model-based results show that alteration in Gq-mediated signaling have short term implications on electrophysiological behavior by linking it through activation of PKC and CaMKII, in consistency with experimental findings (6, 33). Our results predict that each of the two signaling kinases provide distinct regulatory influence on neuronal excitability, suggesting a differential pathway-specific sensitivity of the neuronal circuit controlling blood pressure. Experiemntally observed aberrations in the kinase activities in pathophysiological conditions can be interpreted through our model based approach to understand the effects of AngII on the balance between excitatory and inhibitory effects on sympathetic neurons (34, 46, 47). Opportunies exist for an unbiased approach to identify key sensitivities in the integrated multi-scale network, for example, utilizing global sensitivity analysis and decision trees (78). AngII effects on overall cardiovascular physiology are difficult to predict due to the involvement of AngII signaling in multiple cell types in the control circuit, leading to speculate a "push–pull" hypothesis of AngII action (77). Our integrated model can be extended across multiple cell types to explore the network balances in computationally testing the "push–pull" hypothesis towards explaining the nonlinear effects of AngII on sympathoexcitation as well as sympathoinhibition (20, 21, 87).

A key characteristic of our model is the inclusion of a highly detailed signaling cascade, validated with experimental data from neurons (19). Building on models that consider instantaneous parameter perturbations to simulate the effects of neuromodulators on downstream targets, we examined the effects of signaling kinetics on firing rate dynamics. Simulations support the hypothesis that dynamic neuromodulation is critical for AngII-mediated excitability dynamics, which cannot be captured by simulating neuromodulation as steady state or step reductions of the K_{DR} conductance. Overall, our modeling work suggests that the dynamic interplay between neuromodulatory influences, ionic conductances, and membrane potential determine neuromodulator response in a nonlinear fashion.

Our modeling approach can be expanded to address several physiological questions. Simulations of subthreshold membrane dynamics and synaptic integration can be performed to study the neuromodulation of excitatory and inhibitory input processing. Neuromodulator effects on neural circuits can be studied using our model as a basis for simulating individual cells. The combination of signaling pathway activity with electrophysiology can be integrated into morphologically detailed neuronal models which incorporate experimentally determined spatial variations in channel distributions (88, 89). Our model can also be integrated with AngII signaling-induced transcriptional regulatiory networks to bridge neuromodulation of signaling and electrophysiology with gene expression (78). In the context of autonomic regulation of cardiovascular control, our model could be expanded to study the mechanisms and consequences of aberrant AngII signaling in brainstem neurons from hypertensive rats, based on extensive data on signaling activity and electrophysiological responses to AngII in spontaneously hypertensive rats (47, 90–92). Hence, our multiscale model of integrated signaling and electrophysiology offers broader utility as a platform for studies of neuromodulatory mechanisms underlying physiological function.

ACKNOWLEDGMENTS

This study was supported by NIGMS R01 GM083108 and NHLBI R01 HL111621.

References

1. Marder, E., 2012. Neuromodulation of Neuronal Circuits: Back to the Future. Neuron 76:1–11.
2. Levitan, I., 1994. Modulation of ion channels by protein phosphorylation and dephosphorylation. Annual review of physiology 56:193–212.
3. Finkel, L., 2000. Neuroengineering models of brain disease. Annual review of biomedical engineering 2:577–606.
4. Lu, D., H. Yang, and M. K. Raizada, 1996. Angiotensin II regulation of neuromodulation: downstream signaling mechanism from activation of mitogen-activated protein kinase. The Journal of Cell Biology 135:1609–1617.
5. Lu, D., H. Yang, R. H. Lenox, and M. K. Raizada, 1998. Regulation of angiotensin II-induced neuromodulation by MARCKS in brain neurons. The Journal of Cell Biology 142:217–227.
6. Sumners, C., M. Fleegal, and M. Zhu, 2002. Angiotensin AT1 receptor signalling pathways in neurons. Clinical and experimental pharmacology & physiology 29:483–490.
7. Temporal, S., M. Desai, O. Khorkova, G. Varghese, A. Dai, D. J. Schulz, and J. Golowasch, 2012. Neuromodulation independently determines correlated channel expression and conductance levels in motor neurons of the stomatogastric ganglion. Journal of Neurophysiology 107:718–727.
8. Fellous, J., and C. Linster, 1998. Computational Models of Neuromodulation. Neural Computation 10:771–805.
9. Saucerman, J. J., L. L. Brunton, A. P. Michailova, and A. D. McCulloch, 2003. Modeling beta-adrenergic control of cardiac myocyte

contractility in silico. The Journal of Biological Chemistry 278:47997–48003.
10. Tao, T., D. J. Paterson, and N. P. Smith, 2011. A model of cellular cardiac-neural coupling that captures the sympathetic control of sinoatrial node excitability in normotensive and hypertensive rats. Biophysical Journal 101:594–602.
11. Dolan, A. T., and S. L. Diamond, 2014. Systems modeling of Ca(2+) homeostasis and mobilization in platelets mediated by IP3 and store-operated Ca(2+) entry. Biophysical Journal 106:2049–2060.
12. Fridlyand, L. E., and L. H. Philipson, 2011. Coupling of metabolic, second messenger pathways and insulin granule dynamics in pancreatic beta-cells: a computational analysis. Progress in Biophysics and Molecular Biology 107:293–303.
13. Salvucci, M., Z. Neufeld, and P. Newsholme, 2013. Mathematical model of metabolism and electrophysiology of amino acid and glucose stimulated insulin secretion: in vitro validation using a -cell line. PloS One 8:e52611.
14. Touyz, R., Q. Pu, G. He, X. Chen, G. Yao, M. Neves, and E. Viel, 2002. Effects of low dietary magnesium intake on development of hypertension in stroke-prone spontaneously hypertensive rats: role of reactive oxygen species. Journal of hypertension 20:2221–2232.
15. McCubbin, J., R. DeMoura, I. Page, and F. Olmsted, 1965. Arterial hypertension elicited by subpressor amounts of angiotensin. Science (New York, NY) 149:1394–1395.
16. Hogarty, D., E. Speakman, V. Puig, and M. Phillips, 1992. The role of angiotensin, AT1 and AT2 receptors in the pressor, drinking and vasopressin responses to central angiotensin. Brain research 586:289–294.
17. Phillips, M., and C. Sumners, 1998. Angiotensin II in central nervous system physiology. Regulatory peptides 78:1–11.
18. Ferguson, A., D. Washburn, and K. Latchford, 2001. Hormonal and neurotransmitter roles for angiotensin in the regulation of central autonomic function. Experimental biology and medicine (Maywood, NJ) 226:85–96.
19. Mishra, J., and U. Bhalla, 2002. Simulations of Inositol Phosphate Metabolism and Its Interaction with InsP3-Mediated Calcium Release. Biophysical Journal 83:1298–1316.
20. Accorsi-Mendonca, D., and B. Machado, 2013. Synaptic transmission of baro- and chemoreceptors afferents in the NTS second order neurons. Autonomic neuroscience: basic & clinical 175:3–8.
21. Guyenet, P., 2006. The sympathetic control of blood pressure. Nature reviews. Neuroscience 7:335–346.
22. Thrasher, T., 2006. Arterial baroreceptor input contributes to long-term control of blood pressure. Current hypertension reports 8:249–254.
23. Shan, Z., J. Zubcevic, P. Shi, J. Jun, Y. Dong, T. Murca, G. Lamont, A. Cuadra, W. Yuan, Y. Qi, Q. Li, J. Paton, M. Katovich, C. Sumners, and M. Raizada, 2013. Chronic knockdown of the nucleus of the solitary tract AT1 receptors increases blood inflammatory-endothelial progenitor cell ratio and exacerbates hypertension in the spontaneously hypertensive rat. Hypertension 61:1328–1333.
24. Zubcevic, J., J. Jun, G. Lamont, T. Murca, P. Shi, W. Yuan, F. Lin, J. Carvajal, Q. Li, C. Sumners, M. Raizada, and Z. Shan, 2013. Nucleus of the solitary tract (pro)renin receptor-mediated antihypertensive effect involves nuclear factor-B-cytokine signaling in the spontaneously hypertensive rat. Hypertension 61:622–627.
25. Cuadra, A., Z. Shan, C. Sumners, and M. Raizada, 2010. A current view of brain renin-angiotensin system: Is the (pro)renin receptor the missing link? Pharmacology & therapeutics 125:27–38.
26. Paton, J., S. Wang, J. Polson, and S. Kasparov, 2008. Signalling across the blood brain barrier by angiotensin II: novel implications for neurogenic hypertension. Journal of molecular medicine (Berlin, Germany) 86:705–710.
27. Fernandez, S., M. Huang, B. Davidson, r. Knight, P, and J. Izzo, J, 2003. Modulation of angiotensin II responses in sympathetic neurons by cytosolic calcium. Hypertension 41:56–63.
28. Fernandez, S., M. Huang, B. Davidson, r. Knight, P, and J. Izzo, J, 2005. Mechanisms of angiotensin II-mediated decreases in intraneuronal Ca2+ in calcium-loaded stellate ganglion neurons. Hypertension 45:276–282.
29. Monck, J., R. Williamson, I. Rogulja, S. Fluharty, and J. Williamson, 1990. Angiotensin II effects on the cytosolic free Ca2+ concentration in N1E-115 neuroblastoma cells: kinetic properties of the Ca2+ transient measured in single fura-2-loaded cells. Journal of neurochemistry 54:278–287.
30. Li, Y., and P. Guyenet, 1996. Angiotensin II decreases a resting K+ conductance in rat bulbospinal neurons of the C1 area. Circulation research 78:274–282.
31. Zhu, M., R. Neubig, S. Wade, P. Posner, C. Gelband, and C. Sumners, 1997. Modulation of K+ and Ca2+ currents in cultured neurons by an angiotensin II type 1a receptor peptide. The American journal of physiology 273:C1040–1048.
32. Richards, E., M. Raizada, C. Gelband, and C. Sumners, 1999. Angiotensin II type 1 receptor-modulated signaling pathways in neurons. Molecular neurobiology 19:25–41.
33. Sun, C., C. Sumners, and M. Raizada, 2002. Chronotropic action of angiotensin II in neurons via protein kinase C and CaMKII. Hypertension 39:562–566.
34. Wong, L., J. Polson, D. Murphy, J. Paton, and S. Kasparov, 2002. Genetic and pharmacological dissection of pathways involved in the angiotensin II-mediated depression of baroreflex function. FASEB journal 16:1595–1601.
35. Gelband, C., J. Warth, H. Mason, M. Zhu, J. Moore, J. Kenyon, B. Horowitz, and C. Sumners, 1999. Angiotensin II type 1 receptor-mediated inhibition of K+ channel subunit kv2.2 in brain stem and hypothalamic neurons. Circulation research 84:352–359.
36. Pan, S., C. Sumners, and C. Gelband, 2000. Kv1.4 underlies angiotensin II-mediated inhibition of neuronal A-type K+ current. In Biophysical Journal. Biophysical Society, (Bethesda, MD), volume 78, 450A–450A.
37. Pan, S., M. Zhu, M. Raizada, C. Sumners, and C. Gelband, 2001. ANG II-mediated inhibition of neuronal delayed rectifier K+ current: role of protein kinase C-alpha. American journal of physiology. Cell physiology 281:C17–23.
38. Wang, D., C. Gelband, C. Sumners, and P. Posner, 1997. Mechanisms underlying the chronotropic effect of angiotensin II on cultured

neurons from rat hypothalamus and brain stem. Journal of neurophysiology 78:1013–1020.
39. Wang, D., C. Sumners, P. Posner, and C. Gelband, 1997. A-type K+ current in neurons cultured from neonatal rat hypothalamus and brain stem: modulation by angiotensin II. Journal of neurophysiology 78:1021–1029.
40. Blackwell, K. T., and J. Jedrzejewska-Szmek, 2013. Molecular mechanisms underlying neuronal synaptic plasticity: systems biology meets computational neuroscience in the wilds of synaptic plasticity. Wiley Interdisciplinary Reviews: Systems Biology and Medicine 5:717–731.
41. Bhalla, U. S., 2003. Understanding complex signaling networks through models and metaphors. Progress in Biophysics and Molecular Biology 81:45–65.
42. Ferrante, M., K. T. Blackwell, M. Migliore, and G. A. Ascoli, 2008. Computational Models of Neuronal Biophysics and the Characterization of Potential Neuropharmacological Targets. Current medicinal chemistry 15:2456–2471.
43. Ajay, S. M., and U. S. Bhalla, 2004. A role for ERKII in synaptic pattern selectivity on the time-scale of minutes. European Journal of Neuroscience 20:2671–2680.
44. Bhalla, U. S., 2004. Signaling in Small Subcellular Volumes. II. Stochastic and Diffusion Effects on Synaptic Network Properties. Biophysical Journal 87:745–753.
45. Rybak, I., J. Paton, and J. Schwaber, 1997. Modeling neural mechanisms for genesis of respiratory rhythm and pattern. I. Models of respiratory neurons. Journal of neurophysiology 77:1994–2006.
46. Seyedabadi, M., A. K. Goodchild, and P. M. Pilowsky, 2001. Differential Role of Kinases in Brain Stem of Hypertensive and Normotensive Rats. Hypertension 38:1087–1092.
47. Sun, C., J. Du, C. Sumners, and M. K. Raizada, 2003. PI3-Kinase Inhibitors Abolish the Enhanced Chronotropic Effects of Angiotensin II in Spontaneously Hypertensive Rat Brain Neurons. Journal of Neurophysiology 90:3155–3160.
48. Hines, M. L., T. Morse, M. Migliore, N. T. Carnevale, and G. M. Shepherd, 2004. ModelDB: A Database to Support Computational Neuroscience. Journal of Computational Neuroscience 17:7–11.
49. Yang, H., D. Lu, G. Vinson, and M. Raizada, 1997. Involvement of MAP Kinase in Angiotensin II-Induced Phosphorylation and Intracellular Targeting of Neuronal AT1 Receptors. The Journal of Neuroscience 17:1660–1669.
50. Ouali, R., M. Berthelon, M. Bgeot, and J. Saez, 1997. Angiotensin II receptor subtypes AT1 and AT2 are down-regulated by angiotensin II through AT1 receptor by different mechanisms. Endocrinology 138:725–733.
51. Athanasiades, A., J. Clark, J, F. Ghorbel, and A. Bidani, 2000. An ionic current model for medullary respiratory neurons. Journal of computational neuroscience 9:237–257.
52. Iwamoto, T., S. Wakabayashi, and M. Shigekawa, 1995. Growth factor-induced phosphorylation and activation of aortic smooth muscle Na+/Ca2+ exchanger. The Journal of biological chemistry 270:8996–9001.
53. Iwamoto, T., T. Watano, and M. Shigekawa, 1996. A Novel Isothiourea Derivative Selectively Inhibits the Reverse Mode of Na+/Ca2+ Exchange in Cells Expressing NCX1. Journal of Biological Chemistry 271:22391–22397.
54. Philipson, K., D. Nicoll, M. Ottolia, B. Quednau, H. Reuter, S. John, and Z. Qiu, 2002. The Na+/Ca2+ exchange molecule: an overview. Annals of the New York Academy of Sciences 976:1–10.
55. Hodgkin, A., and A. Huxley, 1952. A quantitative description of membrane current and its application to conduction and excitation in nerve. The Journal of physiology 117:500–544.
56. Peretz, T., G. Levin, O. Moran, W. Thornhill, D. Chikvashvili, and I. Lotan, 1996. Modulation by protein kinase C activation of rat brain delayed-rectifier K+ channel expressed in Xenopus oocytes. FEBS letters 381:71–76.
57. Fakler, B., and J. Adelman, 2008. Control of K(Ca) channels by calcium nano/microdomains. Neuron 59:873–881.
58. Taylor, A., J. Goaillard, and E. Marder, 2009. How multiple conductances determine electrophysiological properties in a multicompartment model. The Journal of Neuroscience 29:5573–5586.
59. Zhu, M., C. Gelband, P. Posner, and C. Sumners, 1999. Angiotensin II decreases neuronal delayed rectifier potassium current: role of calcium/calmodulin-dependent protein kinase II. Journal of neurophysiology 82:1560–1568.
60. Shieh, C., M. Coghlan, J. Sullivan, and M. Gopalakrishnan, 2000. Potassium Channels: Molecular Defects, Diseases, and Therapeutic Opportunities. Pharmacological Reviews 52:557–594.
61. Hille, B., 1994. Modulation of ion-channel function by G-protein-coupled receptors. Trends in Neurosciences 17:531–536.
62. Dayan, P., 2012. Twenty-Five Lessons from Computational Neuromodulation. Neuron 76:240–256.
63. Nadim, F., and D. Bucher, 2014. Neuromodulation of neurons and synapses. Current opinion in neurobiology 29C:48–56.
64. Suh, B.-C., L. F. Horowitz, W. Hirdes, K. Mackie, and B. Hille, 2004. Regulation of KCNQ2/KCNQ3 Current by G Protein Cycling The Kinetics of Receptor-mediated Signaling by Gq. The Journal of General Physiology 123:663–683.
65. Hille, B., E. Dickson, M. Kruse, and B. Falkenburger, 2014. Dynamic metabolic control of an ion channel. Progress in Molecular Biology and Translational Science 123:219–247.
66. Zhou, J., M. S. Shapiro, and B. Hille, 1997. Speed of Ca2+ channel modulation by neurotransmitters in rat sympathetic neurons. Journal of Neurophysiology 77:2040–2048.
67. Blackwell, K. T., 2013. Approaches and tools for modeling signaling pathways and calcium dynamics in neurons. Journal of Neuroscience Methods 220:131–140.
68. Kotaleski, J. H., and K. T. Blackwell, 2010. Modelling the molecular mechanisms of synaptic plasticity using systems biology approaches. Nature Reviews Neuroscience 11:239–251.
69. Bhalla, U. S., 2011. Multiscale interactions between chemical and electric signaling in LTP induction, LTP reversal and dendritic

excitability. Neural Networks 24:943–949.
70. Cortassa, S., M. A. Aon, B. O'Rourke, R. Jacques, H.-J. Tseng, E. Marban, and R. L. Winslow, 2006. A Computational Model Integrating Electrophysiology, Contraction, and Mitochondrial Bioenergetics in the Ventricular Myocyte. Biophysical Journal 91:1564–1589.
71. Saucerman, J. J., and D. M. Bers, 2008. Calmodulin mediates differential sensitivity of CaMKII and calcineurin to local Ca2+ in cardiac myocytes. Biophysical Journal 95:4597–4612.
72. Grandi, E., S. V. Pandit, N. Voigt, A. J. Workman, D. Dobrev, J. Jalife, and D. M. Bers, 2011. Human Atrial Action Potential and Ca2+ Model Sinus Rhythm and Chronic Atrial Fibrillation. Circulation Research 109:1055–1066.
73. Jafri, M. S., and J. Keizer, 1995. On the roles of Ca2+ diffusion, Ca2+ buffers, and the endoplasmic reticulum in IP3-induced Ca2+ waves. Biophysical Journal 69:2139–2153.
74. Stutzmann, G. E., and M. P. Mattson, 2011. Endoplasmic Reticulum Ca2+ Handling in Excitable Cells in Health and Disease. Pharmacological Reviews 63:700–727.
75. Sharpe, L. G., and L. W. Swanson, 1974. Drinking induced by injections of angiotensin into forebrain and mid-brain sites of the monkey. The Journal of Physiology 239:595–622.
76. Ma, X., K. Bielefeldt, Z. Y. Tan, C. A. Whiteis, V. Snitsarev, F. M. Abboud, and M. W. Chapleau, 2006. Dual mechanisms of angiotensin-induced activation of mouse sympathetic neurones. The Journal of Physiology 573:45–63.
77. Dampney, R. A. L., P. S. P. Tan, M. J. Sheriff, M. A. P. Fontes, and J. Horiuchi, 2007. Cardiovascular effects of angiotensin II in the rostral ventrolateral medulla: The push-pull hypothesis. Current Hypertension Reports 9:222–227.
78. Miller, G., B. Ogunnaike, J. Schwaber, and R. Vadigepalli, 2010. Robust dynamic balance of AP-1 transcription factors in a neuronal gene regulatory network. BMC systems biology 4:171.
79. Clark, A. J., T. Balla, M. R. Jones, and K. J. Catt, 1992. Stimulation of early gene expression by angiotensin II in bovine adrenal glomerulosa cells: roles of calcium and protein kinase C. Molecular Endocrinology (Baltimore, Md.) 6:1889–1898.
80. Misonou, H., D. Mohapatra, E. Park, V. Leung, D. Zhen, K. Misonou, A. Anderson, and J. Trimmer, 2004. Regulation of ion channel localization and phosphorylation by neuronal activity. Nature neuroscience 7:711–718.
81. Hagiwara, K., K. Nunoki, K. Ishii, T. Abe, and T. Yanagisawa, 2003. Differential inhibition of transient outward currents of Kv1.4 and Kv4.3 by endothelin. Biochemical and biophysical research communications 310:634–640.
82. Allen, A. M., R. A. Dampney, and F. A. Mendelsohn, 1988. Angiotensin receptor binding and pressor effects in cat subretrofacial nucleus. The American Journal of Physiology 255:H1011–1017.
83. Averill, D. B., T. Tsuchihashi, M. C. Khosla, and C. M. Ferrario, 1994. Losartan, nonpeptide angiotensin II-type 1 (AT1) receptor antagonist, attenuates pressor and sympathoexcitatory responses evoked by angiotensin II and L-glutamate in rostral ventrolateral medulla. Brain Research 665:245–252.
84. Hirooka, Y., P. D. Potts, and R. A. L. Dampney, 1997. Role of angiotensin II receptor subtypes in mediating the sympathoexcitatory effects of exogenous and endogenous angiotensin peptides in the rostral ventrolateral medulla of the rabbit. Brain Research 772:107–114.
85. Khan, R., R. Vadigepalli, M. McDonald, R. Rogers, G. Gao, and J. Schwaber, 2008. Dynamic transcriptomic response to acute hypertension in the nucleus tractus solitarius. American Journal of Physiology. Regulatory, Integrative and Comparative Physiology 295:R15–R27.
86. Park, J., A. Brureau, K. Kernan, A. Starks, S. Gulati, B. Ogunnaike, J. Schwaber, and R. Vadigepalli, 2014. Inputs drive cell phenotype variability. Genome Research 24:930–941.
87. Sheriff, M. J., M. A. P. Fontes, S. Killinger, J. Horiuchi, and R. A. L. Dampney, 2006. Blockade of AT1 receptors in the rostral ventrolateral medulla increases sympathetic activity under hypoxic conditions. American Journal of Physiology - Regulatory, Integrative and Comparative Physiology 290:R733–R740.
88. Ascoli, G. A., K. M. Brown, E. Calixto, J. P. Card, E. J. Galvn, T. Perez-Rosello, and G. Barrionuevo, 2009. Quantitative morphometry of electrophysiologically identified CA3b interneurons reveals robust local geometry and distinct cell classes. The Journal of Comparative Neurology 515:677–695.
89. Ascoli, G. A., S. Gasparini, V. Medinilla, and M. Migliore, 2010. Local control of postinhibitory rebound spiking in CA1 pyramidal neuron dendrites. The Journal of Neuroscience: The Official Journal of the Society for Neuroscience 30:6434–6442.
90. Matsuura, T., H. Kumagai, A. Kawai, H. Onimaru, M. Imai, N. Oshima, K. Sakata, and T. Saruta, 2002. Rostral Ventrolateral Medulla Neurons of Neonatal Wistar-Kyoto and Spontaneously Hypertensive Rats. Hypertension 40:560–565.
91. Sun, C., J. Zubcevic, J. W. Polson, J. T. Potts, C. Diez-Freire, Q. Zhang, J. F. R. Paton, and M. K. Raizada, 2009. Shift to an involvement of phosphatidylinositol 3-kinase in angiotensin II actions on nucleus tractus solitarii neurons of the spontaneously hypertensive rat. Circulation Research 105:1248–1255.
92. Kumagai, H., N. Oshima, T. Matsuura, K. Iigaya, M. Imai, H. Onimaru, K. Sakata, M. Osaka, T. Onami, C. Takimoto, T. Kamayachi, H. Itoh, and T. Saruta, 2012. Importance of rostral ventrolateral medulla neurons in determining efferent sympathetic nerve activity and blood pressure. Hypertension Research 35:132–141.

SUPPLEMENTARY MATERIAL

An online supplement to this article can be found by visiting BJ Online at http://www.biophysj.org.

Supporting Material

Multiscale model of dynamic neuromodulation integrating neuropeptide induced signaling pathway activity with membrane electrophysiology

Hirenkumar K. Makadia[1,†], Warren D. Anderson[1,2,†], Dirk Fey[3,†], Thomas Sauter[4], James S. Schwaber[1], and Rajanikanth Vadigepalli[1,*]

[1]Daniel Baugh Institute for Functional Genomics and Computational Biology, Department of Pathology, Anatomy and Cell Biology, Sidney Kimmel Medical College, Thomas Jefferson University, Philadelphia, PA, USA
[2]Graduate program in Neuroscience, Thomas Jefferson University, Philadelphia, PA, USA
[3]Systems Biology Ireland, University College Dublin, Dublin, Ireland
[4]University of Luxembourg, Life Sciences Research Unit, Luxembourg, Luxembourg

[†]These authors contributed equally to this work.
[*]Correspondence: Rajanikanth.Vadigepalli@jefferson.edu.

S1 Material balance of cytosolic calcium

Intracellular Ca^{2+} levels in the model were modulated by calcium currents (I_{Ca_L} and I_{NaCa}), in addition to a capacitive Ca^{2+} entry to the ER, a membrane calcium pump, and Ca^{2+} buffering processes in the ER (Figure 2A). Excess Ca^{2+} in intracellular levels is transported to ER and stored in Ca^{2+} buffer, which is released by IP3R activation. The mass balance of intracellular (cytosolic) Ca^{2+} is given by

$$\frac{d[Ca^{2+}{}_{cyt}]}{dt} = \underbrace{\frac{I_{NaCa} - I_{Ca_L}}{z v_{cell} F} - r_{Epump}}_{\text{Extracellular}} + \underbrace{N \cdot [\text{CaBuffer}]_T \left(k_{ER}^{Ca^{2+}} \cdot [Ca^{2+}{}_{cyt}] \cdot (1 - [\text{CaBuffer}]_B) - k_{-ER}^{Ca^{2+}} \cdot [\text{CaBuffer}]_B \right)}_{\text{Endoplasmic Reticulum}} \tag{1}$$

where I_{NaCa} is the NCX current, I_{Ca_L} is the L-type calcium channel current , $z(=2)$ is valency of Ca^{2+} ion, F is the Faraday's constant, v_{cell} is the soma volume, r_{Epump} is the rate of Ca^{2+} transfer through extracellular pump, $N(=40)$ is the number of binding sites on CaBuffer, $[\text{CaBuffer}]_T$ is the total concentration of Ca^{2+} buffer in ER , $[\text{CaBuffer}]_B$ is the concentration of bounded Ca^{2+} buffer in ER, $k_{ER}^{Ca^{2+}}$ is the inward rate of Ca^{2+} flux to the ER, and $k_{-ER}^{Ca^{2+}}$ is the outward rate of Ca^{2+} flux from the ER.

S2 Electrophysiology model details

We modeled neurophysiology with an electrical circuit (Figure 1B) containing multiple ionic currents balanced across the membrane as shown in eqs. (2) to (5)

$$C\frac{dV}{dt} = -\sum_i g_i(V)\,(V - E_i) \tag{2}$$

$$g_i(V) = \bar{g}_i \cdot m_i^{M_i}(V) \cdot h_i^{H_i}(V) \tag{3}$$

$$\tau_{m,i}\frac{dm_i}{dt} = m_{\infty,i} - m_i \;; \qquad \tau_{h,i}\frac{dh_i}{dt} = h_{\infty,i} - h_i \tag{4}$$

$$m_{\infty,i} = \left(1 + \exp\left(-\frac{V - V_{1/2,m,i}}{k_{m,i}}\right)\right)^{-x} \;; \qquad h_{\infty,i} = \left(1 + \exp\left(\frac{V - V_{1/2,h,i}}{k_{h,i}}\right)\right)^{-x} \tag{5}$$

where C is the membrane capacitance; V is the voltage across the membrane; and for each ion channel i, g_i is the conductance, E_i is the reversal potential, $\bar{g}_i$ is the maximal conductance, m_i is the activation variable, h_i is the inactivation variable, and M_i and H_i are suitable parameters that are dependent on the kinetics of the channel activation/inactivation.

The time-varying membrane potential-dependent functions $m_i(V)$, $h_i(V)$ in eq. (4) are typically described using nonlinear functions (e.g., $m_{\infty,i} = f(V)$) depending on the paramterized form of Boltzmann functions characterized by half-activation voltage, $V_{1/2}$ and activation curve slope factor, k.

For channels characterized by the Hodgkin-Huxley formalism, the gating variable (p_i, analogous to m_i and h_i) is based on the probability of an individual gate being in a permissive state. Thus $(1 - p_i)$ is the probability of a non-permissive state. The transition between these states is described by first order kinetics:

$$\frac{dp_i}{dt} = \alpha_i(V)(1 - p_i) - \beta_i(V)p_i \tag{6}$$

in which α_i and β_i are voltage-dependent rate constants describing the "non-permissive to permissive" and "permissive to non-permissive" transition rates, respectively. The time course for approaching the equilibrium value of the gating variable ($p_{\infty,i}$) can be described by a τ_i term. The resulting expressions used for solving eq. (6) are:

$$p_{\infty,i} = \frac{\alpha_i(V)}{\alpha_i(V) + \beta_i(V)} \qquad \tau_{p,i} = \frac{1}{\alpha_i(V) + \beta_i(V)} \tag{7}$$

In our modified model, K_{DR} activation was represented by a fourth order Boltzmann function ($x = 4$ in eq. (5)) based on experimental data from rat brain thalamic relay neurons [1]. The half activation voltage was set to 2.3 mV based on voltage-clamp data from brainstem neurons [2]. Our electrophysiology model was simulated as a single compartment (Figure 1B) with the following properties [3]: cell area = 0.0025 mm^2, membrane capacitance $C_m = 1$ uF/cm^2, and E_{leak} was set to maintain baseline firing rates at approximately 1.1 Hz in all simulations.

S3 Calcium baseline-dependent dampening of electrophysiological responses to AngII

We found that the baseline firing rate was elevated in the high Ca^{2+} baseline state (Figure S2A). This finding is consistent with elevated levels of active PKC and CaMKII leading to increased levels of K_{DR} phosphorylation and coincident reduction in hyperpolarizing drive. The excitability response for the high Ca^{2+} baseline condition was smaller and slower than that of the low Ca^{2+} baseline response. However, the steady state firing rates ($t = 300$ s) for high and low Ca^{2+} states were nearly identical, indicating that AngII normalizes the firing rates of cells with divergent Ca^{2+} baseline levels. To determine the electrophysiological basis of the observed excitability differences, we first examined membrane potential traces before and after applying AngII (Figure S2B). Membrane potentials during inter-spike intervals were at approximately -50 mV for both Ca^{2+} baseline conditions. Action potential waveforms and thresholds were also similar for high and low Ca^{2+} baseline states, both before and after applying AngII (Figure S2C). These results suggest that subtle differences in ionic currents during inter-spike intervals account for the Ca^{2+} baseline-dependent differences in firing rates.

To assess the ionic contributions to the membrane potential during inter-spike intervals, we examined membrane potential and current waveforms mediated by Na^+, K_{DR}, and K_{AHP} channels during intervals between APs (K_A and Ca_L currents were omitted because these did not vary in our simulations) (Figure S2D). For the high Ca^{2+} baseline state, firing rates were faster but the membrane potential was more hyperpolarized between APs. The high Ca^{2+} baseline state showed reduced Na^+ and K_{DR} currents along with increased K_{AHP} current between APs, compared to the low Ca^{2+} baseline state. These results are consistent with increased excitability in the high Ca^{2+} baseline states associated with enhanced Na^+ recovery from inactivation (Figure S3). Following AngII application, excitability properties were nearly identical for the low and high Ca^{2+} baseline states. This suggests that AngII drives divergent Ca^{2+} baseline neuronal conditions to a comparable electrophysiological state.

Table S1: **List of signaling pathway models.**

No.	Signaling pathway models	Initial parameter Ref.
1	Gq pathway activation	[4–6]
2	PLCβ hydrolysis	[4]
3	IP3 3-kinase activation	[4]
4	I(145)P3 dephosphorylation	[4]
5	I(1345)P4 dephosphorylation	[4]
6	Multiple inositol polyphosphate phosphatase	[4]
7	Interactions between Inositol high polyphosphates	[4]
8	Dynamics of IP4 interactions	[4]
9	I(134)P3 dephosphorylation	[4]
10	Calcium regulation	[3, 4, 7–11]
11	Calcium binding to calmodulin	[4]
12	CaMKII activation	[4, 12]
13	Protein kinase C activation	[4, 7, 12, 13]

Table S2: **Calcium regulation model. A schematic of the model is shown in Figure 2A.**

Modulation	Reaction	Parameters	Ref.
Calcium transport to ER	$2\,Ca^{2+}_{cyt} + CaTransp \underset{k_b}{\overset{k_f}{\rightleftharpoons}} CaTransp{-}2Ca^{2+}$	$k_f = 3600\ \mu M^{-2}s^{-1};\ k_b = 144\ s^{-1}$	[4]
	$CaTransp{-}2Ca^{2+} \xrightarrow{k_f} CaTransp + 2Ca^{2+}_{seq}$	$k_f = 25\ s^{-1}$	
	$Ca^{2+}_{seq} + CaTransp \underset{k_b}{\overset{k_f}{\rightleftharpoons}} CaTransp + Ca^{2+}_{cyt}$	$k_f = 8\ s^{-1};\ k_b = 8\ s^{-1}$	
Calcium buffer	$5\,Ca^{2+}_{seq} + Cabuffer \underset{k_b}{\overset{k_f}{\rightleftharpoons}} Cabuffer{-}5Ca^{2+}$	$k_f = 0.000489\ \mu M^{-5}s^{-1};\ k_b = 1\ s^{-1}$	[4]
	$5\,Ca^{2+}_{seq} + Cabuffer{-}5Ca^{2+} \underset{k_b}{\overset{k_f}{\rightleftharpoons}} Cabuffer{-}10Ca^{2+}$	$k_f = 0.000489\ \mu M^{-5}s^{-1};\ k_b = 1\ s^{-1}$	
	$5\,Ca^{2+}_{seq} + Cabuffer{-}10Ca^{2+} \underset{k_b}{\overset{k_f}{\rightleftharpoons}} Cabuffer{-}15Ca^{2+}$	$k_f = 0.000489\ \mu M^{-5}s^{-1};\ k_b = 1\ s^{-1}$	
	$5\,Ca^{2+}_{seq} + Cabuffer{-}15Ca^{2+} \underset{k_b}{\overset{k_f}{\rightleftharpoons}} Cabuffer{-}20Ca^{2+}$	$k_f = 0.000489\ \mu M^{-5}s^{-1};\ k_b = 1\ s^{-1}$	
	$5\,Ca^{2+}_{seq} + Cabuffer{-}20Ca^{2+} \underset{k_b}{\overset{k_f}{\rightleftharpoons}} Cabuffer{-}25Ca^{2+}$	$k_f = 0.000489\ \mu M^{-5}s^{-1};\ k_b = 1\ s^{-1}$	
	$5\,Ca^{2+}_{seq} + Cabuffer{-}25Ca^{2+} \underset{k_b}{\overset{k_f}{\rightleftharpoons}} Cabuffer{-}30Ca^{2+}$	$k_f = 0.000489\ \mu M^{-5}s^{-1};\ k_b = 1\ s^{-1}$	
	$5\,Ca^{2+}_{seq} + Cabuffer{-}30Ca^{2+} \underset{k_b}{\overset{k_f}{\rightleftharpoons}} Cabuffer{-}35Ca^{2+}$	$k_f = 0.000489\ \mu M^{-5}s^{-1};\ k_b = 1\ s^{-1}$	
	$5\,Ca^{2+}_{seq} + Cabuffer{-}35Ca^{2+} \underset{k_b}{\overset{k_f}{\rightleftharpoons}} Cabuffer{-}40Ca^{2+}$	$k_f = 0.000489\ \mu M^{-5}s^{-1};\ k_b = 1\ s^{-1}$	
Capacitive calcium entry to ER	$Ca^{2+}_{seq} + Capacitive{-}Ca_{active} \underset{k_b}{\overset{k_f}{\rightleftharpoons}} Capacitive{-}Ca_{inactive}$	$k_f = 0.6912\ \#^{-1}s^{-1};\ k_b = 6.25\ s^{-1}$	[4]
Calcium extracellular pump	$Ca^{2+}_{cyt} + CaEpump \underset{k_b}{\overset{k_f}{\rightleftharpoons}} CaEpump{-}Ca^{2+}$	$k_f = 1800\ \mu M^{-1}s^{-1};\ k_b = 288\ s^{-1}$	[4]
	$CaEpump{-}Ca^{2+} \xrightarrow{k_f} Ca^{2+}_{ext}$	$k_f = 72\ s^{-1}$	
	$Ca^{2+}_{ext} + CaEpump_{leak} \underset{k_b}{\overset{k_f}{\rightleftharpoons}} CaEpump_{leak} + Ca^{2+}_{cyt}$	$k_f = 0.2\ s^{-1};\ k_b = 0.2\ s^{-1}$	
	$Ca^{2+}_{ext} + CapacitiveChannel \underset{k_b}{\overset{k_f}{\rightleftharpoons}} CapacitiveChannel + Ca^{2+}_{cyt}$	$k_f = 0.01\ s^{-1};\ k_b = 0.01\ s^{-1}$	
IP3R activation	$IP3R + 3\,IP3{-}143 \underset{k_b}{\overset{k_f}{\rightleftharpoons}} IP3R_{active}$	$k_f = 0.05\ \mu M^{-3}s^{-1};\ k_b = 1\ s^{-1}$	[4]
	$Ca^{2+}_{seq} + IP3R_{active} \underset{k_b}{\overset{k_f}{\rightleftharpoons}} IP3R_{active} + Ca^{2+}_{cyt}$	$k_f = 3125\ s^{-1};\ k_b = 3125\ s^{-1}$	
Sodium-calcium exchanger	$r_{NaCa} = r_o \cdot m_{GHK} \cdot m_{chemical}$ $m_{chemical} = -\left(1 + \frac{K_{PKCmod}}{1+\exp\left(\frac{K_{PKC}-100[PKC]-3}{D_{PKC}}\right)}\right)\left(\frac{[Ca^{2+}_{cyt}]}{k_m+[Ca^{2+}_{cyt}]}\right)\left(\frac{[Ca^{2+}_{cyt}]}{NaCa_{act}+[Ca^{2+}_{cyt}]}\right)$ $m_{GHK} = -\frac{\left([Ca^{2+}_{ext}][Na^{+}_{cyt}]^3\exp(\gamma\zeta)\right) - \left([Ca^{2+}_{cyt}][Na^{+}_{ext}]^3\exp((\gamma-1)\zeta)\right)}{1+D_{NaCa}\left([Ca^{2+}_{cyt}][Na^{+}_{ext}]^3 - [Ca^{2+}_{ext}][Na^{+}_{cyt}]^3\right)}$		[8–11]

r_{NaCa} = total Ca^{2+} flux, r_o = nominal flux gradient, m_{GHK} = electro-chemical flux across NCX, and $m_{chemical}$ = chemical gradient
$K_{PKCmod} = 0.5$, $K_{PKC} = 10$, $D_{PKC} = 2$, $k_m = 2$, $NaCa_{act} = 0.2$
$\gamma = 0.5$, $\zeta = \frac{zV_mF}{RT}$, $z = 2$, $F = 96500$ C mol^{-1}, $T = 310$ K, $R = 8314$ J kg^{-1} mol$^{-1}K^{-1}$, $D_{NaCa} = 0.05$ nM^{-4}

cyt – cytosolic; seq – sequestered; ext – extracellular; and V_m – membrane potential

Table S3: **Equations for the voltage dependence and kinetic current for brainstem neurons.**

	Current		Expression	Ref.
I_{Na}	$\bar{g}_{\mathrm{Na}} \cdot m_{\mathrm{Na}}^3 \cdot h_{\mathrm{Na}} \cdot (E_{\mathrm{Na}} - V)$	$m_{\infty \mathrm{Na}}$	$\frac{0.091 \cdot (V+38)/(1-\exp(-(V+38)/5))}{0.091 \cdot (V+38)/(1-\exp(-(V+38)/5)) + 0.062 \cdot (V+38)/(\exp((V+38)/5)-1)}$	[3]
		$\tau_{m\mathrm{Na}}$	$(1/(0.091 \cdot (V+38)))/(1-\exp(-(V+38)/5)) + 0.062 \cdot (V+38)/(\exp(V+38)/5) - 1)$	
		$h_{\infty \mathrm{Na}}$	$\frac{0.016 \cdot \exp(-(V+55)/15)}{0.016 \cdot \exp(-(V+55)/15) + 2.07/(1+\exp(-(V-17)/21))}$	
		$\tau_{h\mathrm{Na}}$	$1/(0.016 \cdot \exp(-(V+55)/15)) + 2.07/(1+\exp(-(V-17)/21))$	
$I_{\mathrm{K_{DR}}}$	$\bar{g}_{\mathrm{K_{DR}}} \cdot m_{\mathrm{K_{DR}}}^4 \cdot (E_{\mathrm{K}} - V)$	$m_{\infty \mathrm{K_{DR}}}$	$(1+\exp((V_{12}-V)/k))^{-4}$	[1]
		$\tau_{m\mathrm{K_{DR}}}$	$\frac{1}{4} \cdot (1/(\exp((V-81)/25.6)) + \exp((-(V+132)/18)) + 9.9)$	
$I_{\mathrm{K_A}}$	$\bar{g}_{\mathrm{K_A}} \cdot 0.4 \cdot m_{\mathrm{K_A}}^4 \cdot h_{\mathrm{K_A}} \cdot (E_{\mathrm{K}} - V)$	$m_{\infty \mathrm{K_A}}$	$1/(1+\exp(V+36/20))$	[3]
		$\tau_{m\mathrm{K_A}}$	$1/(\exp(V+35.82)/19.69) + \exp(-(V+79.69)/12.7) + 0.37)$	
		$h_{\infty \mathrm{K_A}}$	$1/(1+\exp(V+78/6))$	
		$\tau_{h\mathrm{K_A}}$	$1/(\exp(V+46.05)/5) + \exp(-(V+238.4)/37.45))$ if $V < -63$, else $\tau_{hK_A} = 60.0$	
$I_{\mathrm{K_{AHP}}}$	$\bar{g}_{\mathrm{K_{AHP}}} \cdot m_{\mathrm{K_{AHP}}}^2 \cdot (E_{\mathrm{K}} - V)$	$m_{\infty \mathrm{K_{AHP}}}$	$\frac{1.25 \cdot 10^{-8}[\mathrm{Ca}_{\mathrm{cyt}}^{+2}]^2}{(1.25 \cdot 10^{-8}[\mathrm{Ca}_{\mathrm{cyt}}^{+2}]^2) + 2.5}$	[3, 8]
		$\tau_{m\mathrm{K_{AHP}}}$	$1000/((1.25 \cdot 10^{-8}[\mathrm{Ca}_{\mathrm{cyt}}^{+2}]^2) + 2.5)$	
$I_{\mathrm{Ca_L}}$	$\bar{g}_{\mathrm{Ca_L}} \cdot m_{\mathrm{Ca_L}}^2 \cdot (E_{\mathrm{Ca}} - V)$	$m_{\infty \mathrm{Ca_L}}$	$\frac{1.6/(\exp(-0.072 \cdot (V-5)))}{1.6/(\exp(-0.072 \cdot (V-5))) + (0.02 \cdot (V-1.31)/(\exp((V-1.31)/5.36)-1))}$	[3]
		$\tau_{m\mathrm{Ca_L}}$	$1/(1.6/(\exp(-0.072 \cdot (V-5))) + (0.02 \cdot (V-1.31)/(\exp((V-1.31)/5.36)-1)))$	
I_{leak}	$g_{\mathrm{leak}} \cdot (E_{\mathrm{leak}} - V)$	-		[3]

$$\frac{dV_m}{dt} = \frac{1}{C_m} \cdot (I_{\mathrm{Na}} + I_{\mathrm{K_{DR}}} + I_{\mathrm{K_A}} + I_{\mathrm{K_{AHP}}} + I_{\mathrm{Ca_L}} + I_{\mathrm{leak}})$$

Note that $\mathrm{Ca}_{\mathrm{cyt}}^{2+}$ used in this Table is different from the cytosolic Ca^{2+} in Table S2. See first subsection of the results for details.

I_{Na} – Fast sodium current, $I_{\mathrm{K_{DR}}}$ – Delayed rectifier potassium current, $I_{\mathrm{K_A}}$ – Fast activating potassium current
$I_{\mathrm{K_{AHP}}}$ – Hyperpolarized calcium dependent potassium current, $I_{\mathrm{Ca_L}}$ – High threshold calcium current

Table S4: **Model of phosphorylation of ion-channels through intermediate kinetics.**

Reaction	Rates	Parameters
$\mathrm{K_U} + 4\,\mathrm{PKC} \underset{k_{dp,PKC}}{\overset{k_{p,PKC}}{\rightleftharpoons}} \mathrm{K_{PKC}} + 4\,\mathrm{PKC}$	$k_{p,PKC}[\mathrm{K_U}][\mathrm{PKC}]^4 - k_{dp,PKC}[\mathrm{K_{PKC}}]$	$k_{p,PKC} = 10$; $k_{dp,PKC} = 0.7312$
$\mathrm{K_U} + 4\,\mathrm{CaMKII} \underset{k_{dp,CaMKII}}{\overset{k_{p,CaMKII}}{\rightleftharpoons}} \mathrm{K_{CaMKII}} + 4\,\mathrm{CaMKII}$	$k_{p,CaMKII}[\mathrm{K_U}][\mathrm{CaMKII}]^4 - k_{dp,CaMKII}[\mathrm{K_{CaMKII}}]$	$k_{p,CaMKII} = 1$; $k_{dp,CaMKII} = 3.3215$
$\mathrm{K_{CaMKII}} + 4\,\mathrm{CaMKII} \underset{k_{dp,CaMKII}}{\overset{k_{p,CaMKII}}{\rightleftharpoons}} \mathrm{K_{PKC,CaMKII}} + 4\,\mathrm{CaMKII}$	$k_{p,CaMKII}[\mathrm{K_{PKC}}][\mathrm{CaMKII}]^4 - k_{dp,CaMKII}[\mathrm{K_{PKC,CaMKII}}]$	$k_{p,CaMKII} = 1$; $k_{dp,CaMKII} = 3.3215$
$\mathrm{K_{PKC}} + 4\,\mathrm{PKC} \underset{k_{dp,PKC}}{\overset{k_{p,PKC}}{\rightleftharpoons}} \mathrm{K_{PKC,CaMKII}} + 4\,\mathrm{PKC}$	$k_{p,PKC}[\mathrm{K_{CaMKII}}][\mathrm{PKC}]^4 - k_{dp,PKC}[\mathrm{K_{PKC,CaMKII}}]$	$k_{p,PKC} = 10$; $k_{dp,PKC} = 0.7312$

$\mathrm{K_U}$ – Unphosphorylated potassium ion-channels ($\mathrm{K_{DR}}$), $\mathrm{K_{PKC}}$, $\mathrm{K_{CaMKII}}$ and $\mathrm{K_{PKC,CaMKII}}$ – phosphorylated potassium ion-channels ($\mathrm{K_{DR}}$)

Table S5: **Hill function models of signaling responses to AngII. Peak and steady state responses were separately normalized and fitted as functions of AngII concentration. Value pairs refer to the peak parameter value followed by the steady state parameter value.**

	Low Ca^{2+}		High Ca^{2+}	
	$K_{0.5}$ (nM)	nH	$K_{0.5}$ (nM)	nH
PLC	4.8, 5.51	1.06, 1.21	4.2, 4.3	1.04, 1.04
IP3	11.1, 9.3	1.06, 1.11	9.9, 9.9	1.08, 1.08
PKC	3.4, 3.3	1.07, 1.37	3.8, 3.8	1.03, 1.03
CaMKII	12.6, 12.6	1.59, 1.59	2.4, 2.4	1.51, 1.52

Table S6: **Hill function models of excitability responses to AngII. Peak and steady state responses were separately normalized and fitted as functions of AngII concentration. Value pairs refer to the peak parameter value followed by the steady state parameter value.**

Phenotype	$K_{0.5}$ (nM)	nH
Wildtype	25.6, 26.4	1.55, 1.53
Blocking PKC site	7.8, 6.3	1.09, 1.24
Blocking CaMKII site	4.1, 4.3	1.16, 1.50

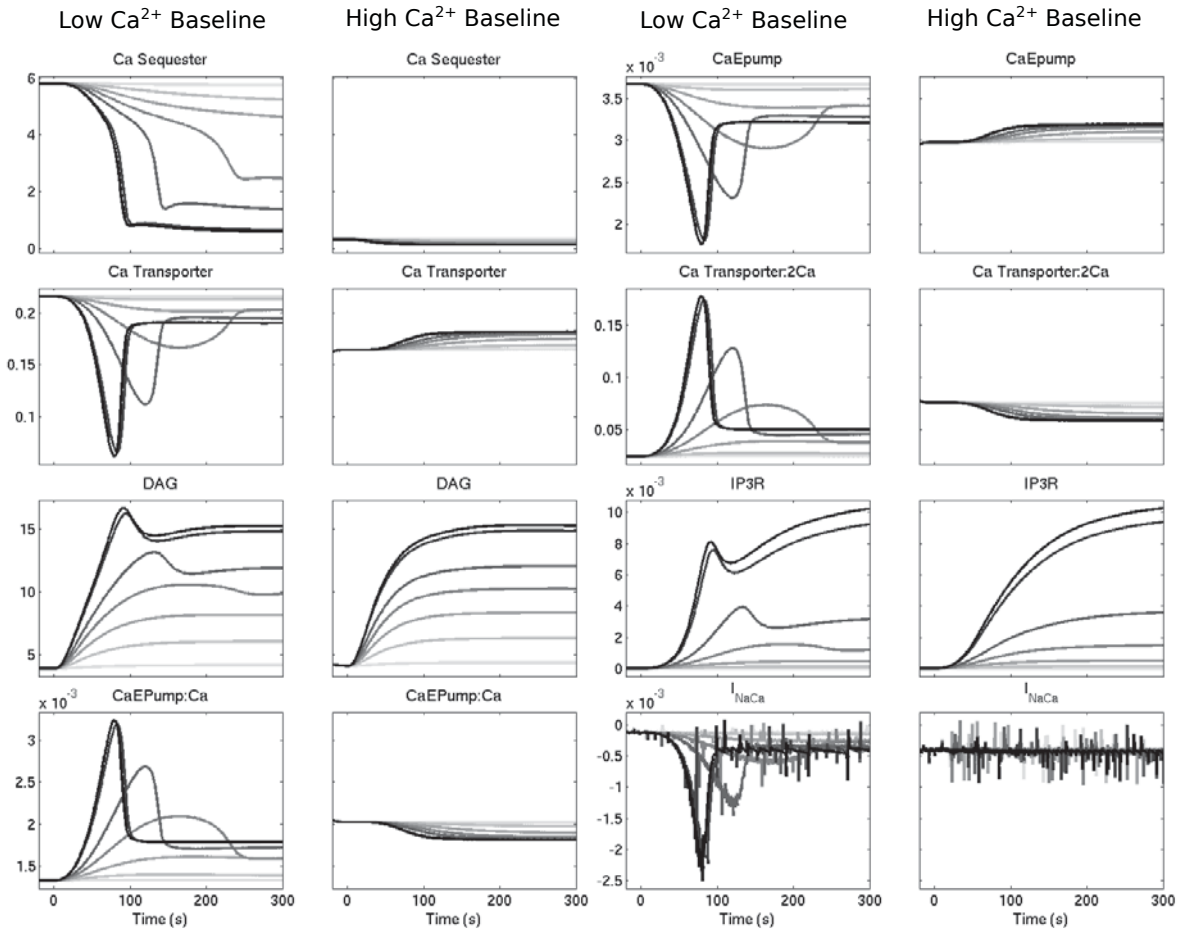

Figure S1: **Additional plots to Figure 2 of AngII elicited responses to different Ca^{2+} baseline conditions.** Low Ca^{2+} baseline and high Ca^{2+} baseline response plots to different doses of AngII for sequestered Ca^{2+}, CaTranp, DAG, CaEpump:Ca, CaEpump, CaTranp:2Ca, IP3R and NCX current (I_{NaCa}).

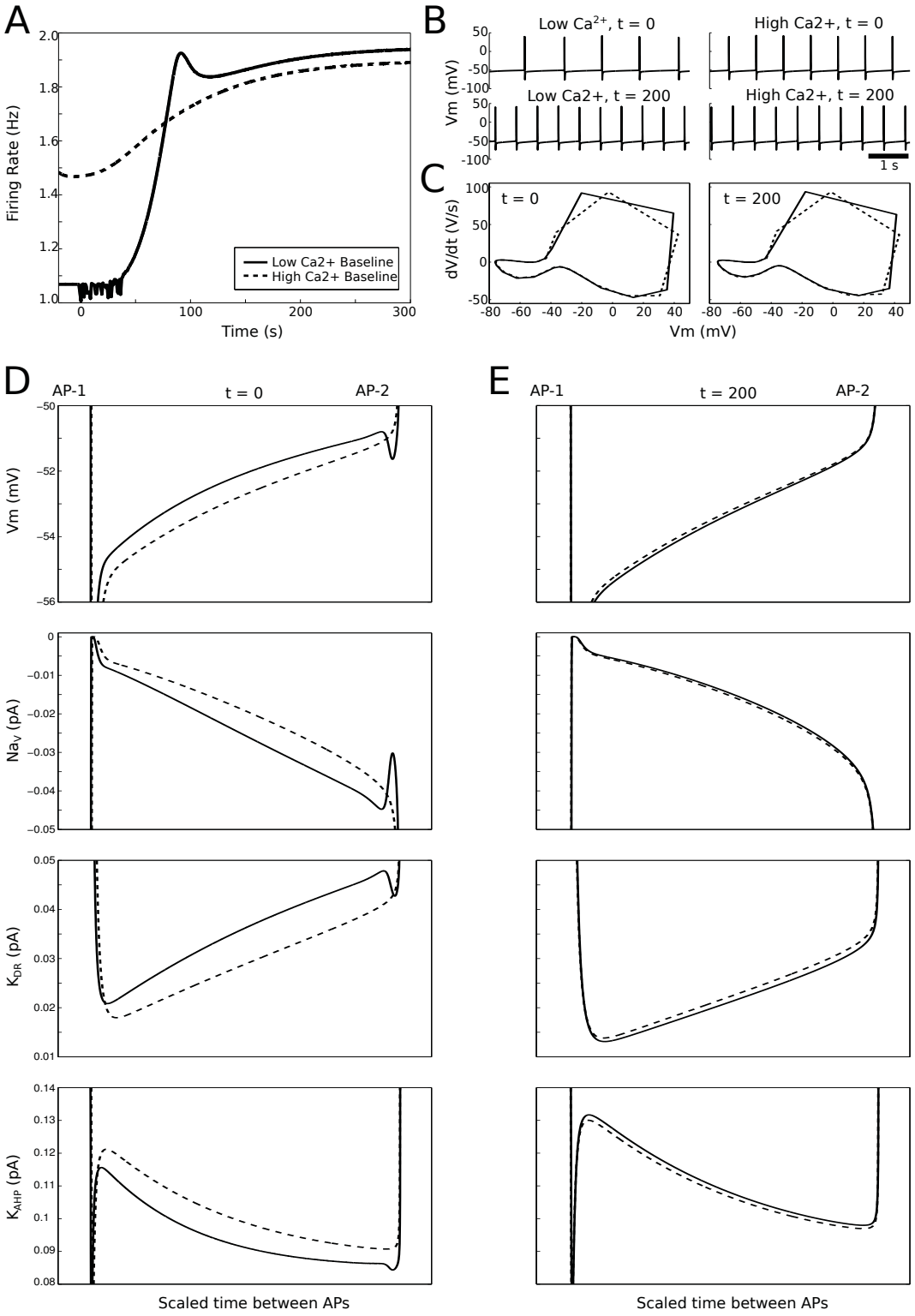

Figure S2: **Low Ca^{2+} baseline neuronal state exhibits a larger increase in AngII-induced excitability.** (A) Firing rate responses to AngII (100 nM at $t = 0$ s) are shown for low and high Ca^{2+} baseline levels. (B) Membrane potential waveforms are shown before ($t = 0$ s) and after ($t = 200$ s) AngII effects have stabilized. (C) Phase-space representations of APs before and after AngII (same legend as in panel A). (D) Biophysical differences between the low and high Ca^{2+} baseline conditions (same legend as in panel A). All data are plotted during normalized time intervals between two APs (AP-1 and AP-2) to show the inter-spike interval properties either before (left, $t = 0$ s) or after (right, $t = 200$ s) AngII stimulation. Abbreviations: Vm = membrane potential, $Na_V = Na^+$ current, $K_{DR} = K_{DR}$ current, $K_{AHP} = K_{AHP}$ current.

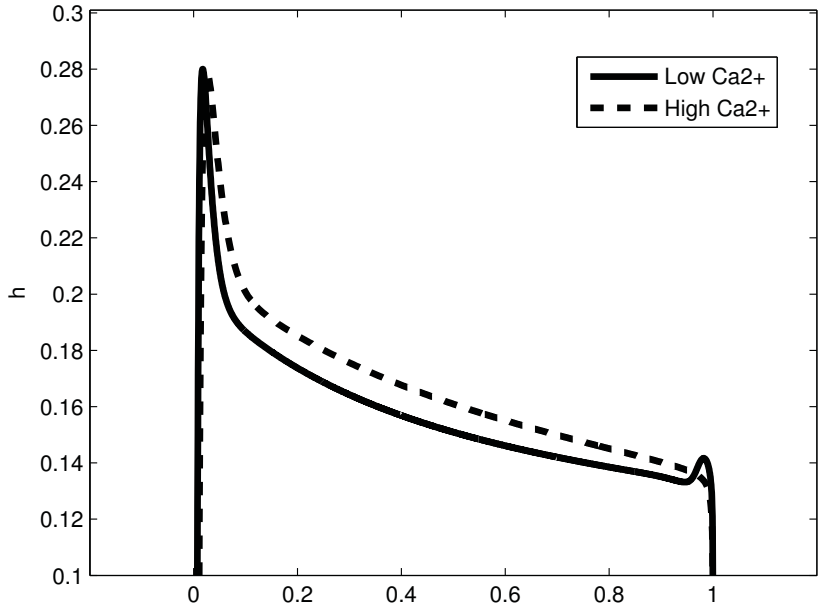

Figure S3: **Inactivation variable (h) for Na^+ channel at steady state for high and low Ca^{2+} baseline states.** Normalized time between two action potentials are represented from 0 to 1 on x–axis.

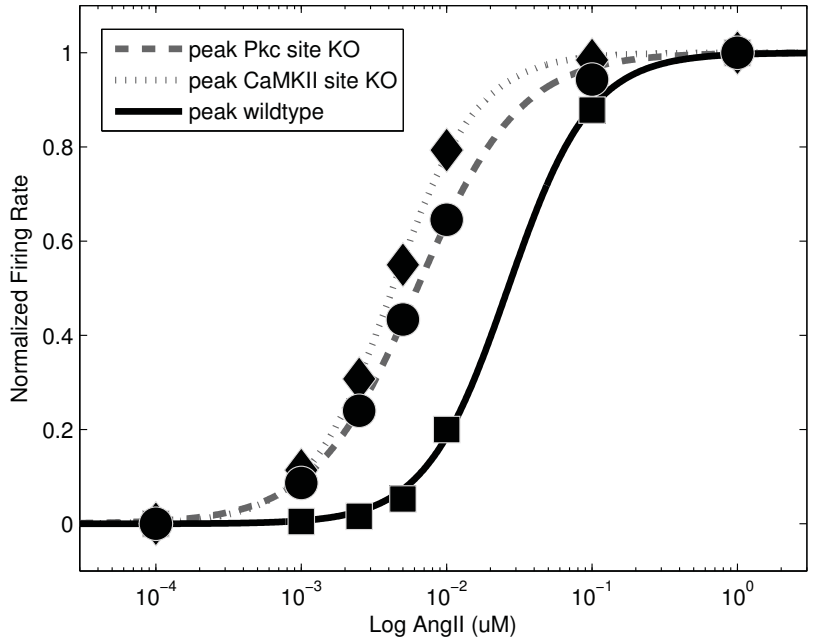

Figure S4: **Peak dose response curves for different blocking conditions of kinases.**

Supporting References

[1] J Huguenard and D Prince. Slow inactivation of a TEA-sensitive K current in acutely isolated rat thalamic relay neurons. *Journal of neurophysiology*, 66(4):1316–1328, 1991.

[2] C Gelband, J Warth, H Mason, M Zhu, J Moore, J Kenyon, B Horowitz, and C Sumners. Angiotensin II type 1 receptor-mediated inhibition of K+ channel subunit kv2.2 in brain stem and hypothalamic neurons. *Circulation research*, 84(3):352–359, 1999.

[3] I Rybak, J Paton, and J Schwaber. Modeling neural mechanisms for genesis of respiratory rhythm and pattern. i. models of respiratory neurons. *Journal of neurophysiology*, 77(4):1994–2006, 1997.

[4] J Mishra and U Bhalla. Simulations of inositol phosphate metabolism and its interaction with InsP3-Mediated calcium release. *Biophysical Journal*, 83(3):1298–1316, 2002.

[5] R Ouali, M Berthelon, M Bégeot, and J Saez. Angiotensin II receptor subtypes AT1 and AT2 are down-regulated by angiotensin II through AT1 receptor by different mechanisms. *Endocrinology*, 138(2):725–733, 1997.

[6] H Yang, D Lu, G Vinson, and M Raizada. Involvement of MAP kinase in angiotensin II-induced phosphorylation and intracellular targeting of neuronal AT1 receptors. *The Journal of Neuroscience*, 17(5):1660–1669, 1997.

[7] S Pan, M Zhu, M Raizada, C Sumners, and C Gelband. ANG II-mediated inhibition of neuronal delayed rectifier K+ current: role of protein kinase C-alpha. *American journal of physiology. Cell physiology*, 281(1):C17–23, 2001.

[8] A Athanasiades, Jr Clark, J, F Ghorbel, and A Bidani. An ionic current model for medullary respiratory neurons. *Journal of computational neuroscience*, 9(3):237–257, 2000.

[9] T Iwamoto, S Wakabayashi, and M Shigekawa. Growth factor-induced phosphorylation and activation of aortic smooth muscle Na+/Ca2+ exchanger. *The Journal of biological chemistry*, 270(15):8996–9001, 1995.

[10] T Iwamoto, T Watano, and M Shigekawa. A novel isothiourea derivative selectively inhibits the reverse mode of Na+/Ca2+ exchange in cells expressing NCX1. *Journal of Biological Chemistry*, 271(37):22391–22397, 1996.

[11] K Philipson, D Nicoll, M Ottolia, B Quednau, H Reuter, S John, and Z Qiu. The Na+/Ca2+ exchange molecule: an overview. *Annals of the New York Academy of Sciences*, 976:1–10, 2002.

[12] M Zhu, C Gelband, P Posner, and C Sumners. Angiotensin II decreases neuronal delayed rectifier potassium current: role of calcium/calmodulin-dependent protein kinase II. *Journal of neurophysiology*, 82(3):1560–1568, 1999.

[13] D Wang, C Sumners, P Posner, and C Gelband. A-type K+ current in neurons cultured from neonatal rat hypothalamus and brain stem: modulation by angiotensin II. *Journal of neurophysiology*, 78(2):1021–1029, 1997.